Author response

We thank the reviewers for their constructive and insightful feedback on our manuscript. Their comments have helped to strengthen the manuscript by clarifying several key points throughout the manuscript and overall have improved the clarity and readability. Below we provide a point-by-point response, with reviewer comments in plain text and our response in red with updates to the manuscript in italics. All the line numbers cited in this response refer to the revised manuscript.

Reviewer 1

The manuscript entitled *"Lagrangian investigation of GCMs during the 2014-15 Holuhraun eruption reveals large differences in the representation of aerosol size distribution"* is well written, clearly presented, and thoroughly documented. I thank the authors for conducting a comprehensive analysis of the selected GCMs and their ability to simulate aerosol transport and PNSD. The methodology is robust, well explained, and sufficiently detailed to allow reproducibility. The results are clearly presented and discussed. Overall, I recommend publication after minor revisions.

Specific Comments

Section 3.1

The authors may consider using the Sulfur Oxidation Ratio (SOR), defined as SO4/(SO2+ SO4). SOR is a commonly used metric to quantify the conversion of SO2 to sulfate and can provide useful insight into sulfur oxidation processes and aerosol aging. It may also help identify environments where aqueous or heterogeneous oxidation pathways are important. A similar analysis could potentially strengthen the discussion associated with Figure 10. Ref-(Rogers, M. J., Joo, T., Hass-Mitchell, T., Canagaratna, M. R., Campuzano-Jost, P., Sueper, D., Tran, M. N., Machesky, J. E., Roscioli, J. R., Jimenez, J. L., Krechmer, J. E., Lambe, A. T., Nault, B. A., and Gentner, D. R.: Humid summers promote urban aqueous-phase production of oxygenated organic aerosol in the northeastern United States, Geophys. Res. Lett., 52, e2024GL112005, https://doi.org/10.1029/2024gl112005, 2025.)

Thank you for this suggestion. We have replaced the total sulphate with the SOR and added the following to the discussion in Section 3.1 to provide further insights into differences in the sulphate oxidation processes between the models:

Lines 726-735:

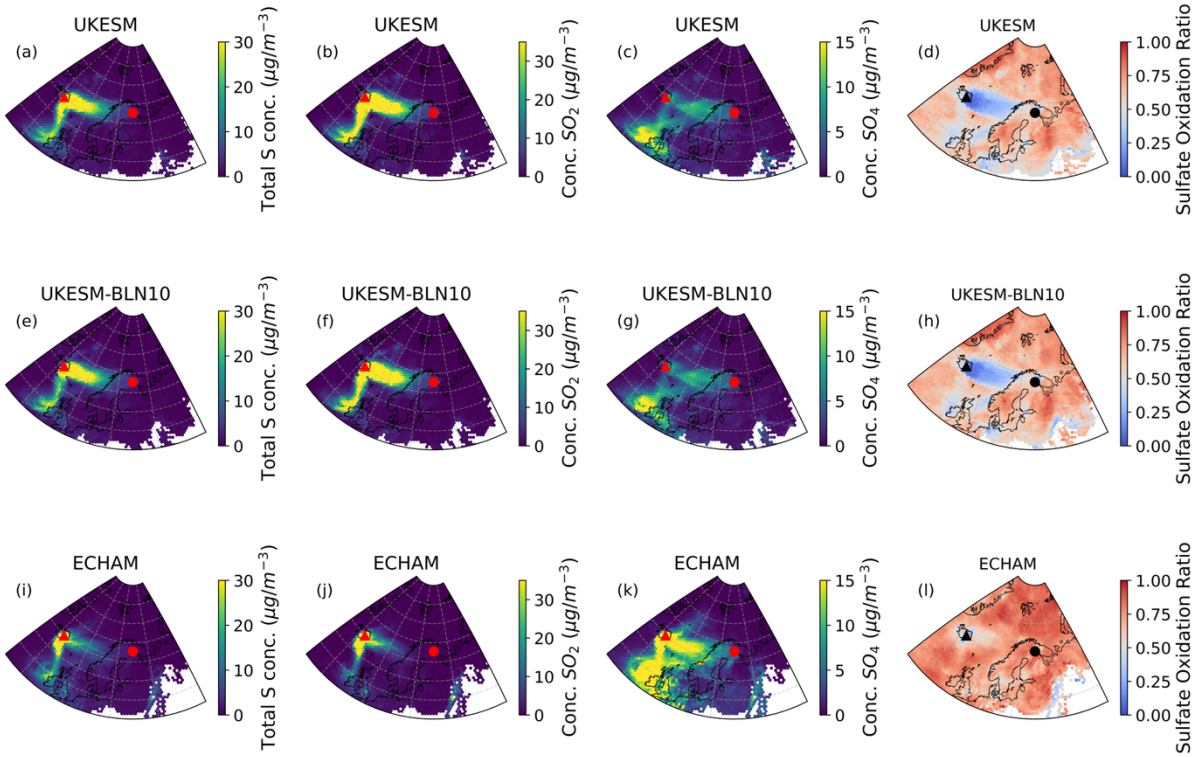


Figure 10: The CVT receptor models (Eq. 3) for total S (a, e and i), SO_2 (b, f and j) and SO_4 (c, g and k) mass concentrations (conc.) collocated along back trajectories from Värriö. As well as the sulfate oxidation ratio of SO_2 to SO_4 (d, h and l). For UKESM1.0 (a-d), UKESM1.0-BLN10 (e-h) and ECHAM6.3-HAM2.3 (i-l). All figures for September 2014.

'The sulphate oxidation ratio (SOR) is an established proxy for sulphate formation defined as $SO_4/(SO_2+ SO_4)$ (Cheng et al., 2016; , Jordan et al. 2024; Rogers et al., 2025; Wang et al., 2016; Wang and Zhang, 2023). This highlights the difference in conversion processes between UKESM and ECHAM. The majority of the sulphate is converted in the vicinity of Iceland for ECHAM (Fig. 10l),whereas, in UKESM, the plume over the Atlantic clearly experiences a large contribution of SO_2 before landfall on Norway (Figs. 10d and 10h).'

In addition, UKESM and UKESM-BLN appear to show similar SO_2 concentrations. How similar are the sulfate concentrations in these two models? Comparing the SOR values between them may help explain differences in sulfate production and the underlying oxidation mechanisms.

Lines 735-757: *'Generally, UKESM and UKESM-BLN show similar SO_2 and SO_4 concentrations (Fig. S18). There are differences in the magnitude of the two defined plumes with lower concentrations in the plume expanding towards the UK, and higher SO_2 concentrations in the plume towards the observational site, but these do not lead to substantial differences in the SOR'*

To facilitate comparison to other studies we also calculate the SO_2-SO_4 ratio. This uses a CVT-like receptor model, using the median of each grid cell, rather than the mean used in the CVT model, to mitigate influence of extremes derived from taking the ratio. Jordan et al. (2024) used an exponential decay relationship to derive the near-vent SO_2-SO_4 ratio of 25 ± 5 using a network of in-situ measurement sites, which agreed with the ratio derived in Ilyinskaya et al., (2017). Boichu et al. (2019) estimated a slightly lower ratio of 19.7 using a linear model. Using the CVT receptor model, the UKESM variants reveal SO_2-SO_4 ratios in the plume over the North Atlantic between ~10-40, with higher values around the vent (approximately 30) for UKESM (Fig. 11a). The slightly higher SO_2/SO_4 ratios near the vent (approximately 35) in UKESM-BLN may suggest a contribution of organic mediation boundary layer nucleation to increasing SO_2 depletion, however as concentrations are mostly consistent it is more likely to be due to slight differences in transport. We find that ECHAM demonstrates

considerably lower ratios across the region considered, with a near vent ratio (of approximately 5) 4-6 times lower than any of these observationally derived estimations (Fig. 10l), and consistent with the underestimation of SO_2 at the measurement sites (Fig. 5). Similarly in Jordan et al. (2024), ECHAM6.3-HAM2.3 was found to have the lowest near-vent SO_2-SO_4 ratio compared to the four other GCMs and chemical transport model (CTM), whereas UKESM1.0 had one of the most comparable SO_2-to-SO_4 ratios to those observed. The Lagrangian analysis undertaken here suggests that this is due to the overly efficient conversion of SO_2-to-SO_4 near the vent in ECHAM.

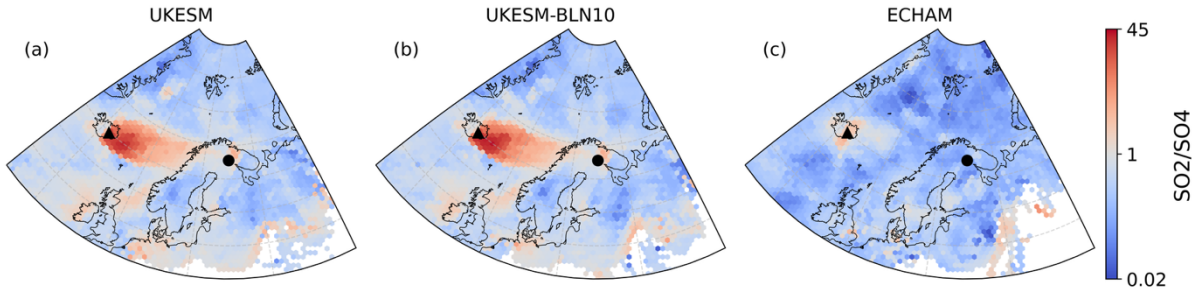


Figure 11: The receptor models equivalent to the CVT model using the median for the ratio of SO2 to SO4 mass concentrations (conc.) collocated along back trajectories from Värriö for UKESM1.0 (a), UKESM1.0-BLN10 (b) and ECHAM6.3-HAM2.3 (c). Note the use of a logarithmic colourbar with ratio equivalent limits. All figures for September 2014.

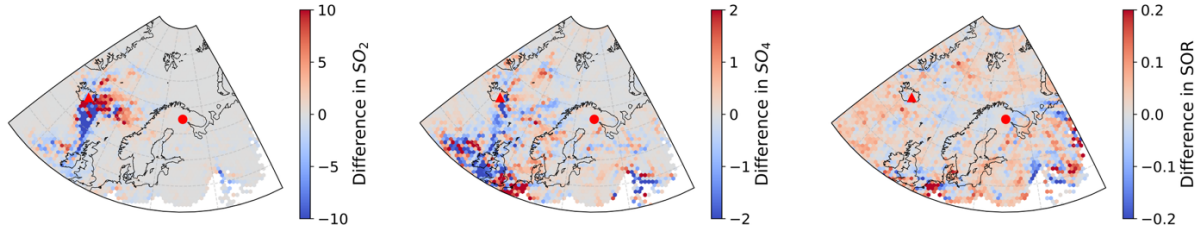


***Figure S18:** Difference between UKESM1.0-BLN10 and UKESM1.0 in CWT receptor models for (a) SO_2 concentration, (b) SO_4 concentration and (c) sulphur oxidation ratio (SOR).*

Figure 6-UKESM-BLN appears to exhibit some signatures of banana-shaped growth patterns, although these features are relatively short-lived. There also seems to be a recurring burst of nucleation during the early morning hours from days 11–16. This repetitive pattern may suggest a role of photochemistry, with increasing oxidant production after sunrise promoting particle formation. It would be interesting if the authors could discuss the dominant mechanisms controlling nucleation in these simulations.

Thank you for your comment, we have added to the discussion of nucleation, describing the dominant mechanisms in the simulations.

***Lines 485-495:** 'The characteristic timing of NPF at Värriö with average event start times located around noon (Jokinen et al., 2022; Vehkamäki et al., 2004), is replicated by the observations with the start of the 'banana' plots at around midday for each observed growth event (Fig. 6a). This reflects the role of photochemistry with increasing oxidant production after sunrise promoting NPF. For both UKESM-BLN and ECHAM the nucleation modes occur throughout the timeseries at approximately midday (Figs. 6c and 6d), highlighting the photosynthetically driven nature of this process, and indicating that the impact of the diurnal cycle on oxidant production is represented. Nucleation rates in the Metzger nucleation scheme depend on both sulfuric acid (H_2SO_4) and organic oxidation products to build up nucleation precursor availability (Metzger et al., 2010), with oxidants interactively simulated in UKESM driven by thermal and photolytic reactions (Sellar et al., 2019). In ECHAM the oxidant fields for OH, H_2O_2, NO_2, and O_3 are monthly mean fields (Stier et al., 2005) prescribed from calculations of the MOZART chemical transport model (Horowitz et al., 2003), onto which the model imposes a diurnal cycle internally; within each day OH follows a cosine profile peaking at local solar noon.'*

Line 575- ECHAM has prescribed oxidants from climatology, do they have a diurnal cycle attached? Can this affect the mechanisms that control NPF?

Thank you this is an important point to highlight, we have added text to describe the diurnal cycle applied to the oxidants within the ECHAM model and the importance of this for representation NPF, linking this to the description of the diurnal cycle in the previous comment, see lines 466-477 above.

We have added to the line previously describing the ECHAM oxidants, to reference back to the discussion of oxidants in Sect. 3.2.:

Lines 758-759: *'ECHAM atmospheric oxidants are prescribed by an 8-year climatology (Inness et al., 2013) as described in Sect. 3.2, whereas for UKESM the oxidants are interactively simulated and depleted by oxidation reactions (Sellar et al., 2019).'*

General Figure Presentation

Several figures could potentially be enlarged for improved readability. Reducing label sizes and using common color bars where appropriate may help maximize the plotting area. For example, in Figure 10, the (DD-MM-YYYY) date labels could potentially be shown only on the bottom row of panels, and the rest of the panels may only account for (DD), allowing more space for the plot. If space permits, including a 100 nm tick mark on the y-axis may also help readers identify the approximate boundary of the Aitken mode.

Thank you for this comment, we have revised the figures to maximise space where possible and added a 100nm tick mark on the size distribution timeseries figures.

Section 3.3 – Figure 10

The observed volcanic PNSD exhibits a bimodal structure, characterized by a pronounced Aitken mode and a secondary accumulation mode. Several models reproduce this behavior, although with varying degrees of uncertainty. Could the authors discuss the physical processes responsible for this bimodal structure? For example, does it reflect a combination of newly formed particles that have grown into the Aitken mode together with condensational growth on pre-existing particles along the transport pathway?

Thank you for noting this, we have updated Section 3.3 to include discussion of the bimodal structure:

Lines 590-603*: 'During the eruption in September 2014 there is a distinct trend across all three sites in the observations: an increase in the modal diameter for the accumulation mode compared to the climatology (Fig. 8a-c). The increase in modal diameter of particles is further highlighted when considering the surface area of particles (dS/dlogDp) (Fig. S16). The averaged size distributions for the eruption period also exhibit a clear bimodal structure with a deepening of the intermodal minimum. For the climatology period, the boreal sites exhibit an average size distribution without a clear bimodal structure separated by a clear Hoppel minima, which is indicative of pristine environments with new particle formation processes as a source of ultrafine particles and condensation growth (Heikkinen et al., 2024). The changes to the size distribution during September 2014 could be associated with the increased availability of precursor gases promoting additional and accelerated condensational growth, as well as condensational growth on to pre-existing particles along the transport pathway. The trough between the Aitken and accumulation mode can also be associated a with cloud-processing induced Hoppel minimum. However, from the clear growth pattens in the size distribution timeseries (Fig. 6a), there is likely a contribution from enhanced growth and condensation in 2014 compared to the climatology period. Pallas demonstrates a decrease in the Aitken mode diameter (Fig. 8b) which is not evident at Värriö, perhaps due to the comparative proximity to the eruption and the time for growth during transport between the sites (Väänänen et al., 2013).'*

Lines 633-641*: 'The growth in accumulation mode and Aitken mode diameter and lack of increase in particle number is suggestive of growth processes such as condensation, coagulation and cloud processing (Figs. 8j and 8k).*

In ECHAM, for cloud portions of model grid volumes, there is complete removal of sulfuric acid gas through condensation, and no aerosol nucleation takes place (Kazil et al., 2010; Zhang et al., 2012). Thus, in-cloud oxidation results in a population of particles with larger mass but not an increase in particle number. In-cloud

processing is also associated with a pronounced Hoppel minimum which is exhibited in the average size distributions for Värriö and Pallas simulated by ECHAM during the eruption period (Figs. 8j and 8k). Contrastingly, the representation of the aerosol size distribution in ECHAM at Zeppelin shows a significant increase in the concentration of nucleation mode particles, suggesting a significant contribution of gas-phase oxidation during transport to this location (Fig. 8l).'

Lines 663-676: '*There is also a deepening of the intermodal minima between the Aitken mode and accumulation mode for the average size distribution during the eruption which is not present in the climatology (Fig. 8g and 8h). The deepening of this trough is reflective of the changes in the observed distribution, likely associated with accelerated new particle growth and condensation under enhanced precursor gases associated with the eruption. However, the effect is much stronger in UKESM-BLN than the in-situ observations. At Zeppelin the response is different: there is a decrease in concentrations for all modes, but an increase at all modal diameters (Fig. 8i). The decrease in Aitken mode concentrations during the eruption simulated by UKESM-BLN is consistent with the observational dataset, however, the change is overestimated. This suggests that the coagulation and growth from the volcanic perturbation leads to an increase in the average Aitken and accumulation mode diameters, and a decrease in particle number concentrations in the Aitken and nucleation modes. The distinct Hoppel minimum in the climatology is lost for the averaged size distribution during the eruption period (Fig. 8i). As regional growth and condensation is not simulated at Zeppelin in UKESM-BLN (Fig. S9c), instead particles must be created earlier in transport, thus elevated coagulation and condensation sinks lead to an overall suppression of nucleation and Aitken mode populations. These relationships are similar to those observed (Fig. 8c), however the effect is too strong in UKESM-BLN (Fig. 8i).'*

In addition, ECHAM appears to show an unusually strong nucleation mode at Zeppelin, which is relatively far from the volcanic source. Could the authors comment on whether this feature reflects a systematic model bias or a specific process represented in the model?

Thanking for this comment we have added the following text to the manuscript to expand on the discussion of the strong nucleation mode simulated in ECHAM at Zeppelin.

Lines 641-648: *'The strong nucleation mode feature has been noted in previous ECHAM-HAM studies of size distribution at Zeppelin (Virtanen et al., 2025a), as well as Leinonen et al., (2022) in which ECHAM6.3-HAM2.3 demonstrated the highest nucleation concentration across all the models considered, overestimating the observations during the summer and September. ECHAM includes charged nucleation, unlike the UKESM variants, which decreases the vapor concentration threshold needed to form new particles. This is particularly significant to pristine regions like the Arctic due to the low concentrations of nucleation precursors. The nucleation concentration bias is exacerbated even further during the eruption period which could be due to the increased availability of sulphate precursors as well as ECHAM having a much lower climatological condensation sink compared to the observations (Figs. 8c and 8l).'*

Line 505-The authors mention a significant contribution from gas-phase oxidation. Could they clarify whether the precursor gases responsible for this oxidation are primarily volcanic in origin, or whether background sulfur species also contribute?

We note that background sulphur species will contribute despite the relatively rural locations selected. There will be influence from anthropogenic sulphur sources as well as natural sources such as DMS. However, this is controlled by to the best of our ability by comparing to a September climatology to represent average background conditions. We acknowledge there will be interannual variability however, the perturbation from the volcano is a substantial addition of sulphur into these environments. We have clarified the text as:

Lines 649-653*: 'We note that despite the rural locations of the stations, and selection of transport regimes associated with the eruption location, sources of sulphur from both local natural and anthropogenic sources, as well as long-range transport, could be associated with interannual variability in aerosol number size distributions (Asmi et al., 2011; Jang et al., 2021). These differences cannot be fully isolated in the comparison between the eruption and climatology.'*

Line 600-How is the contribution from pre-existing sulfate separated from newly formed sulfate? Is the source of sulfate known in this analysis? Clarifying whether the sulfate was already present in the atmosphere or was produced through new particle formation in the volcanic plume and subsequent growth would be helpful.

Thank you for your comment. We acknowledge that there will be background levels of sulphate already present in the atmosphere. To separate the contribution from the background sulphate influence, we have compared to a climatology and isolated transport from the volcano. We have added text to highlight this limitation included in the previous answer (***lines 649-653***).

From the Lagrangian analysis we are able to attribute the plume of sulphate stemming from the volcano in all three model variants (Figs. 10, 11 and 12). In the models this is associated with nucleation particles in both UKESM variants (Figs. 12c and 12f) near the vent and in the plume near the coast of Iceland, as well as over Europe and the UK. Whereas, in ECHAM we note that there are not high nucleation mode concentrations collocated with the sulphur and sulphate plumes from the volcano (Fig. 12i), instead the highest nucleation mode concentrations are associated with regions suggestive of other natural and anthropogenic sources of precursor gases. We have added text to highlight the potential sources of the different areas of high nucleation particle concentrations. We are not able to perform the same analysis for the observations due to the 4D data requirement for the CVT models and the limitations of instrument detection at the smallest diameters for the observations. We have added further discussion of the nucleation mode concentration distribution in section 4.3:

Lines 785-812*: 'The condensation sink spatial distribution in the CVT framework is generally consistent across the three models (Figs. 12a, 12d and 12g). However, in the North Atlantic and West of Iceland, before the plume, ECHAM demonstrates a lower condensation sink (Fig. 12g). Despite the condensation sink being high in the vicinity of the vent, SO_4 levels are high enough to sustain nucleation in UKESM and UKESM-BLN, with evidence of new particles in the plume extending off the coast of Iceland (Figs. 12c and 12f). In ECHAM, despite higher concentrations of SO_4 and a lower condensation sink before the plume, there are much lower concentrations of nucleation sized particles in the plume (Figs. 12g-i). However, there are high concentrations of nucleation mode particles at the eruption site (Fig. 12i). The conversion of SO_2 to SO_4 is much more rapid in ECHAM and happens almost entirely in before the plume reaches the ocean (Fig. 10). When combined with the lack of nucleation particles associated with the eruption in the plume, this suggests condensation and coagulation or growth due to in-cloud oxidation are the dominating mechanisms during transport from the eruption in ECHAM (Fig. 12i).*

Nucleation mode (1-10 nm) concentrations are generally much lower in UKESM compared to the other GCMs (Figs. 10c, 10f and 10i), with high concentrations only found in the region of the North Atlantic closest to the vent. This is consistent with previous studies that have suggested that the binary H_2SO_4-H_2O nucleation scheme is not able to replicate the unusually high formation rate of NPF in volcanic plumes (Boulon et al., 2011). In UKESM-BLN there are high concentrations of nucleation particles close to the vent (Fig. 12f), and the high concentrations associated with the plume extend over a larger area than those associated with the binary neutral homogeneous H_2SO_4-H_2O nucleation in UKESM (Fig. 12c).

Interestingly, the spatial distribution of nucleation particles associated with background conditions is very distinct in UKESM-BLN (Fig. 12f) compared to ECHAM (Fig. 12i). High concentrations of nucleation mode particles are associated with transport over Europe and the UK for UKESM-BLN, likely associated with anthropogenic emissions (e.g. Alam et al., 2003; Bousiotis et al., 2021) in combination with organic mediated BLN over these forested regions. However, in ECHAM nucleation mode particles are associated with transport over the Arctic, likely associated with charged nucleation of sulphuric acid and water which has been found to contribute most significantly (up to 70%) to concentrations of ultrafine aerosol in the BL over high latitude oceans due to cold temperatures and high ionisation rates in these regions (Kazil et al., 2010). The sources of sulphate in the Arctic are likely local natural marine biogenic emissions, such as DMS as well as long-range anthropogenic emissions. These distinct nucleation source regions will result in different aerosol base states for the Holuhraun perturbation, particularly due to the difference in distance of nucleation particle formation from the measurement site, and thus the time for evolution and growth. This has important implications for ACI estimates as the aerosol perturbation impact on cloud properties will depend strongly on the background aerosol population.'

Introduction

It would be useful to provide a brief description of the volcanic emissions. For example:

- What were the major emitted species (SO_2, ash, other gases)?
- What were the estimated injection heights during the eruption?
- Were there significant temporal variations in the eruption characteristics?

Such information would help place the modeling results into context.

Thank you, we have added further detail to the introduction regarding the description of the volcanic emissions:

Lines 39-47: *'Tropospheric plumes from degassing eruptions with low levels of explosivity, are predominantly mixtures of gas and aerosol particulate matter (PM) with low quantities of ash. The Holuhraun eruption released large quantities of volcanic gases into the atmosphere: in total 11 Mt of SO2, 6 Mt CO2, 0.1 Mt HCl and 0.05 Mt HF (Gíslason et al., 2015; McCoy and Hartmann, 2015; Schmidt et al., 2015, Stafansson et al 2017) and sulphate comprised approximately 90% of the PM mass (Ilyinskaya et al., 2017), with the altitude of the centre of mass mainly confined within 0-6 km (Carboni et al. 2019). The young plume had a high gas to particle ratio (Ilyinskaya et al., 2017). The SO_2 emissions peaked in September 2014 with emission rates varying throughout the month: Schmidt et al. (2015) estimated up to 0.12 Tg day^{-1} during early September, 0.02–0.6 Tg day^{-1} between 6 and 22 September and 0.06–0.12 Tg day^{-1} until the end of September and a daily maximum of 0.26 Tg day^{-1}.'*

Minor Comments

- Tables S3 and S4 refer to the "number of empty distributions at start," whereas Table S5 refers to the "percentage of empty distributions." Please clarify whether this difference is intentional or a typographical inconsistency.

Thank you for noting this topographical inconsistency, we have corrected this in the supplementary material.

- Line 373: "other studies have found have" appears a typographical error.

Thank you for noting this error, we have corrected this in the manuscript.

Citation: https://doi.org/10.5194/egusphere-2026-1043-RC1

Reviewer 2

This manuscript uses the 2014–2015 Holuhraun effusive eruption as a natural experiment to examine aerosol microphysical processes in two global climate models, ECHAM6.3-HAM2.3 and UKESM1.0. The study compares in situ particle number size distribution (PNSD) measurements from three rural sites with model output sampled using a Lagrangian trajectory framework. A third simulation, UKESM1.0 with organic-mediated boundary-layer nucleation (UKESM-BLN), is also included to test whether this additional nucleation pathway improves the simulated PNSD evolution during plume transport.

The results suggest that the Holuhraun eruption affected the observed PNSD at all three sites. During the eruption period, the observations show a consistent increase in accumulation-mode diameter and particle growth consistent with new particle formation (NPF) during plume transport. ECHAM6.3-HAM2.3 does not reproduce this sustained growth and appears to attribute much of the response to the growth of pre-existing particles. UKESM1.0 also does not capture the observed increase in modal diameter. UKESM-BLN improves the simulated modal-diameter evolution, but this improvement comes with a substantial overestimate of Aitken-mode number concentrations.

The manuscript is clearly written and the analysis is generally comprehensive. My main concern is that the improvement in UKESM-BLN is interpreted mainly through the presence of the BLN parameterization, without fully diagnosing whether the mechanism is physically consistent with the Holuhraun plume environment. I also have concerns about the use of trajectory clusters to interpret microphysical processes without stronger constraints from meteorological history.

Major comments

1. UKESM-BLN includes organic-mediated boundary-layer nucleation following Metzger et al. (2010), but the Holuhraun perturbation is primarily an SO_2 perturbation. For organic-mediated BLN to be efficient, the model also needs suitable organic vapors, favorable boundary-layer structure, and a condensation sink low enough for newly formed particles to survive. The manuscript should therefore show where and when the UKESM-BLN nucleation is actually active relative to the model-defined boundary layer.

This point is important because boundary-layer NPF can depend strongly on mixed-layer evolution, residual-layer influence, and vertical structure, as shown by Zeppelin-based observations of NPF onset and growth in the planetary boundary layer (Lampilahti et al., 2021). It would be useful to know whether the initial BLN source occurs mainly in the mixed layer, and whether the particles then grow or are transported into the residual layer or entrainment zone. Without this diagnostic, the improved performance of UKESM-BLN should be interpreted cautiously and should not, by itself, be taken as evidence for plume-wide organic-mediated BLN.

Thank you for raising this point. To examine the NPF events in the context of the model-defined boundary layer we included additional analysis focused on defining whether transport was in or out of boundary layer during NPF events. Mixed layer depth is calculated by HYSPLIT during trajectory calculation from the boundary layer height for each model/ reanalysis dataset. We compared the mixed layer depth to trajectory height to calculate whether the trajectories were in or out of boundary layer during the NPF events. We have added this analysis in both a eulerian framework (using the end points of the trajectories at the station) and a lagrangian perspective for UKESM-BLN, looking at NPF events evolution along the trajectories and the fraction of ensemble trajectories in the boundary layer and each point along the 10 day trajectories. Note that the trajectory release height is fixed at each station release location (with ensemble perturbations) (Table 3), so whether the trajectory is in the boundary layer at these points is determined by the mixed layer depth. We have also included the condensation sink on the size distibution timeseries figures to compare the condensation sink before NPF events in each model.

It is important to note that the NPF events are only observed at boreal forest stations in UKESM-BLN, as highlighted by the size difference plots added in Fig. S7. In these regions there will be suitable organic vapours to promote organic mediated boundary layer nucleation and NPF events are expected even without the volcanic perturbation (see timeseries for example a climatology year (2013), Figure A1 below).

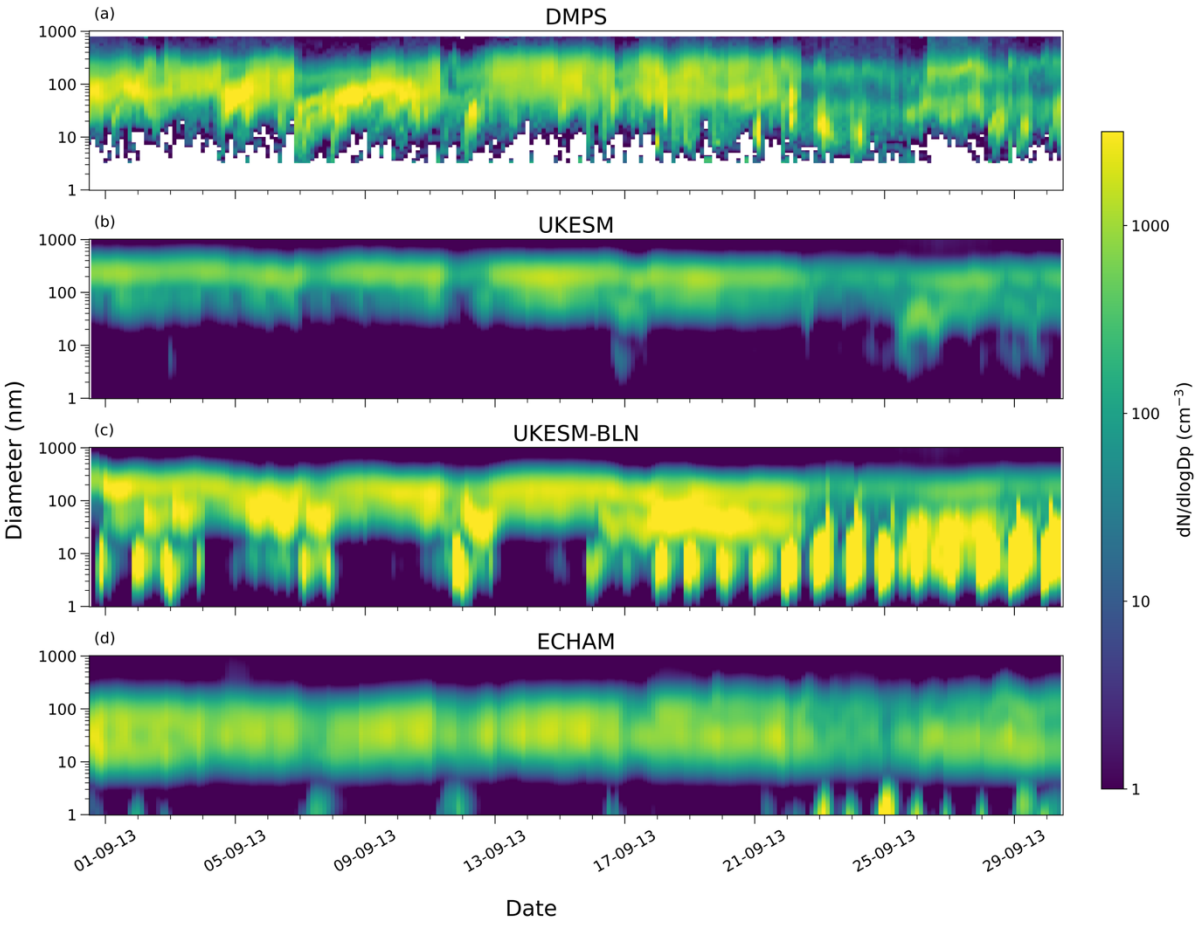


Figure A1: Timeseries of size distribution for September 2013 at Värriö in dN/dlogD$_p$. (a) observations (DMPS), (b) UKESM1.0, (c) UKESM1.0-BLN and (d) ECHAM6.3HAM2.3. Note that the x axis labels and ticks indicate the date at midday.

We have added the following text and updated the figures in the manuscript and supplementary material.

***Lines 496-514**: 'In the boreal forest, UKESM demonstrates a very strong diurnal cycle for the boundary layer height, with shallow boundary layers overnight, and a peak in number of trajectories residing in the boundary layer just before midday (Figs. 6b and 6c). Whilst this sharp diurnal cycle is observed for trajectories calculated from ERA-interim reanalysis (e.g. 16-20th September) (Fig. 6a), the repeated collapse of the nighttime boundary layer is repeated almost every day throughout September 2014 for UKESM (Fig. 6b and 6c). For ECHAM the trajectory endpoints are almost entirely always in the boundary layer (Fig. 6d). The onset of NPF events for UKESM-BLN coincide with the time that all the trajectories are in the boundary layer, when the condensation sink is low for both Värriö (Fig. 6c) and Pallas (Fig. S8). Considering the evolution of NPF in a Lagrangian perspective (Fig. S12) allows us to see the development of the events during the airmass history for UKESM-BLN. Taking trajectories from 12-hourly points during the largest sustained growth event (15-17th of September), demonstrates the regional persistence of these events, continuing with clear sustained growth for almost 45 hours over land before arriving at the station (Fig. S12). The nucleation bursts coincide with air-mass transport within the boundary layer, substantiating that these are indeed boundary layer NPF events in UKESM-BLN, likely associated with organic precursors contributing to or triggering NPF over the boreal forest (Tunved et al. 2006) as well as sulphur emissions from the eruption. The growth rates for the Aitken mode for particularly long lives post-NPF growth events in the observations (15-18th of September and 18th-20th) were calculated finding similar results for UKESM-BLN as in the observations (Table S10). Whilst UKESM which employs the Vehkamäki et al. (2002) nucleation scheme throughout the boundary layer does exhibit bursts of nucleation mode particles (Fig. 6a) and closely matches the observed coagulation sink (10nm) (Fig. S14b) and condensation sink (Fig. S14a), it does not replicate the magnitude or growth stemming from the observations post NPF growth events (Fig. S13a, Table S10), highlighting the importance of the organic-mediated boundary layer nucleation parameterisation.'*

***Lines 547-555**: 'There is no evidence of sustained growth into accumulation mode size ranges following NPF events at Zeppelin, contrasting to the boreal sites in the PNSD timeseries (Fig. S9). Aitken bursts in the observed size distribution coincide with trajectory end points in the boundary layer (Fig. S9), suggesting growth post-NPF events. Observations in September, during the Arctic freeze up, have been found to be associated with contribution from more local sources and boundary layer nucleation contribution to the Aitken mode (Price et al., 2023). Nucleation bursts observed in the size distribution timeseries for all models for Zeppelin coincide frequently with trajectory endpoints outside the boundary layer, implying a free tropospheric contribution to nucleation particles at the site (Fig. S9). These differences also could be due to the role of vertical resolution and the representation of boundary layer, discussed in Sect. 4.1.'*

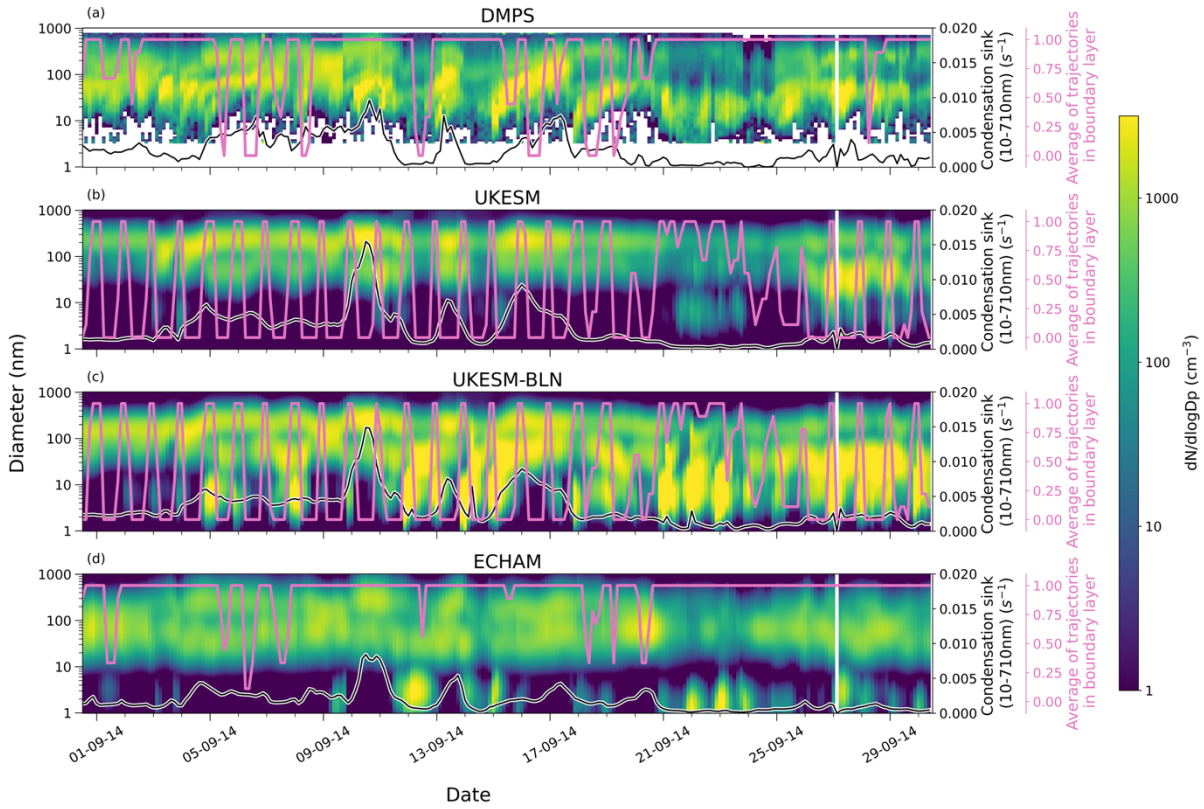


Figure 6: Timeseries of size distribution for September 2014 at Värriö in dN/dlogD_p. (a) observations (DMPS), (b) UKESM1.0, (c) UKESM1.0-BLN and (d) ECHAM6.3HAM2.3. Note that the x axis labels and ticks indicate the date at midday. The black line shows the condensation sink for each timestep and the pink line indicates the fraction of the ensemble back-trajectories in the boundary layer starting at each timestep.

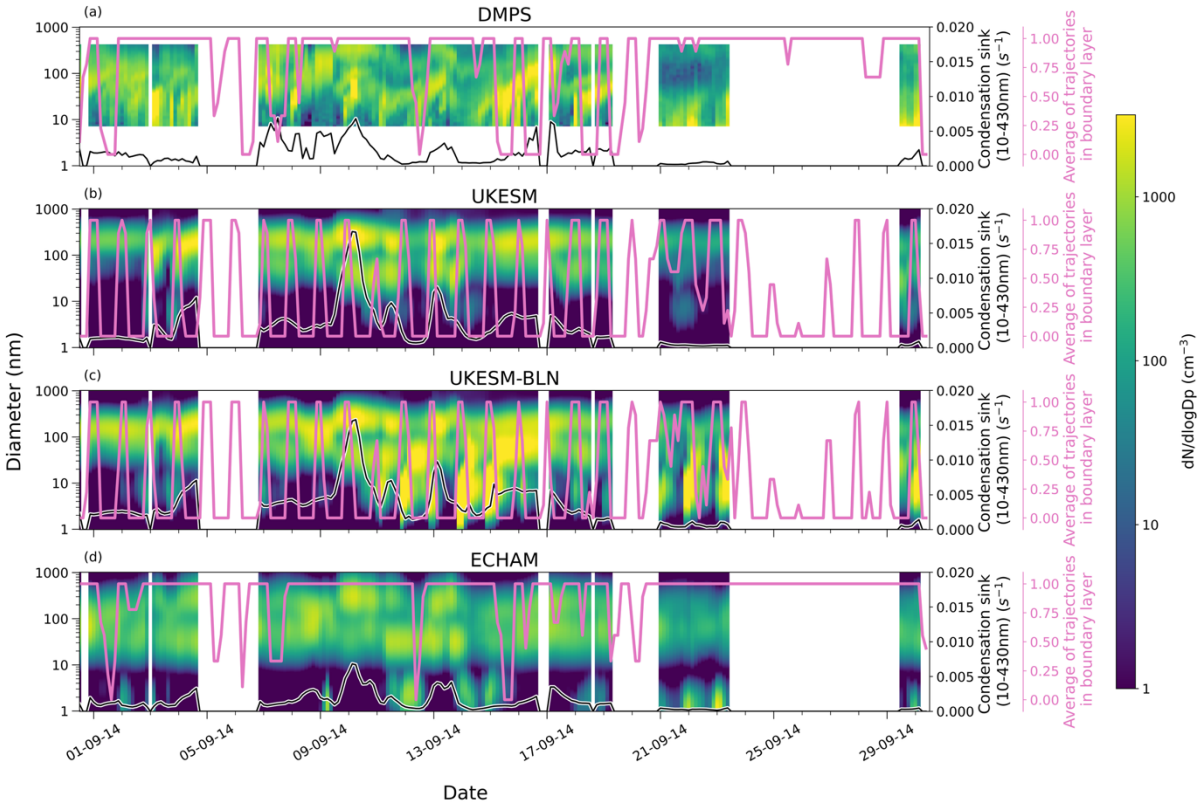


Figure S8: *Timeseries of size distribution for September 2014 at Pallas in dN/dlogD_p. (a) observations (DMPS), (b) UKESM1.0, (c) UKESM1.0-BLN and (d) ECHAM6.3HAM2.3. The black line shows the condensation sink for each timestep and the pink line indicates the fraction of the ensemble back-trajectories in the boundary layer starting at each timestep.*

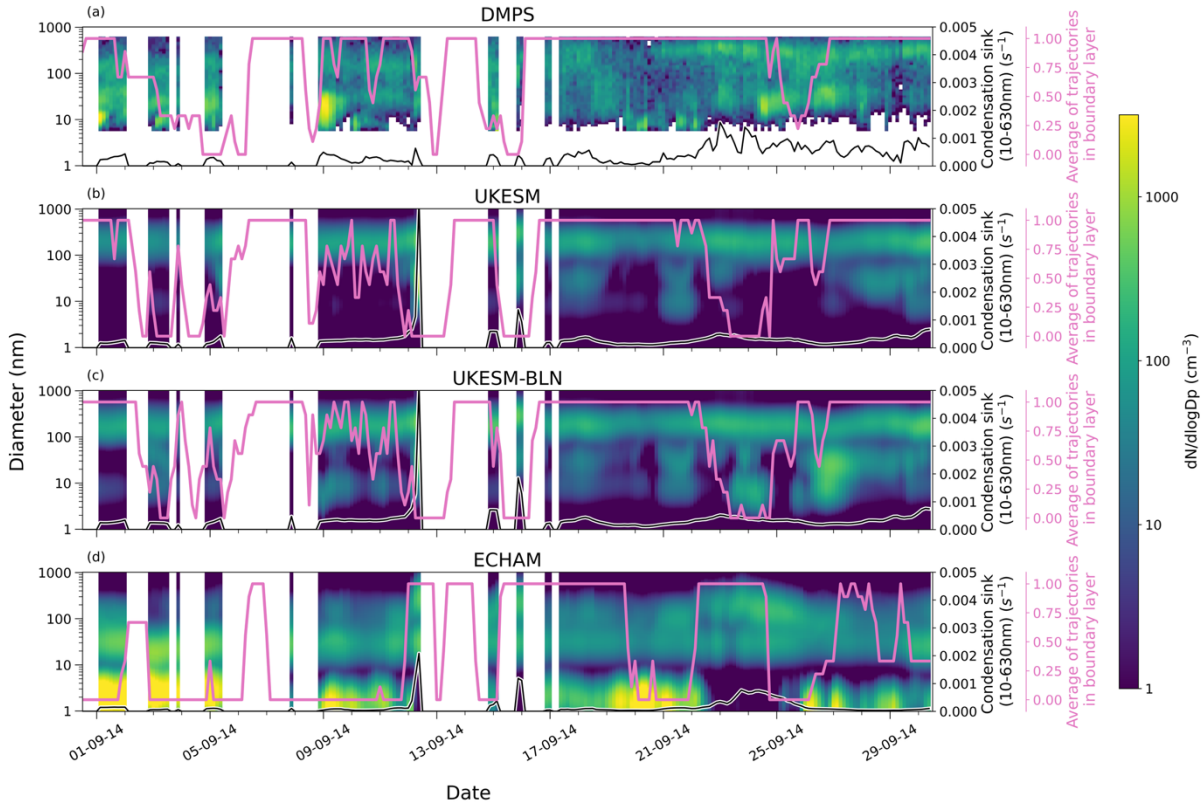


Figure S9: *Timeseries of size distribution for September 2014 at Zeppelin in dN/dlogD_p. (a) observations (DMPS), (b) UKESM1.0, (c) UKESM1.0-BLN and (d) ECHAM6.3HAM2.3. The black line shows the condensation sink for each timestep and the pink line indicates the fraction of the ensemble back-trajectories in the boundary layer starting at each timestep.*

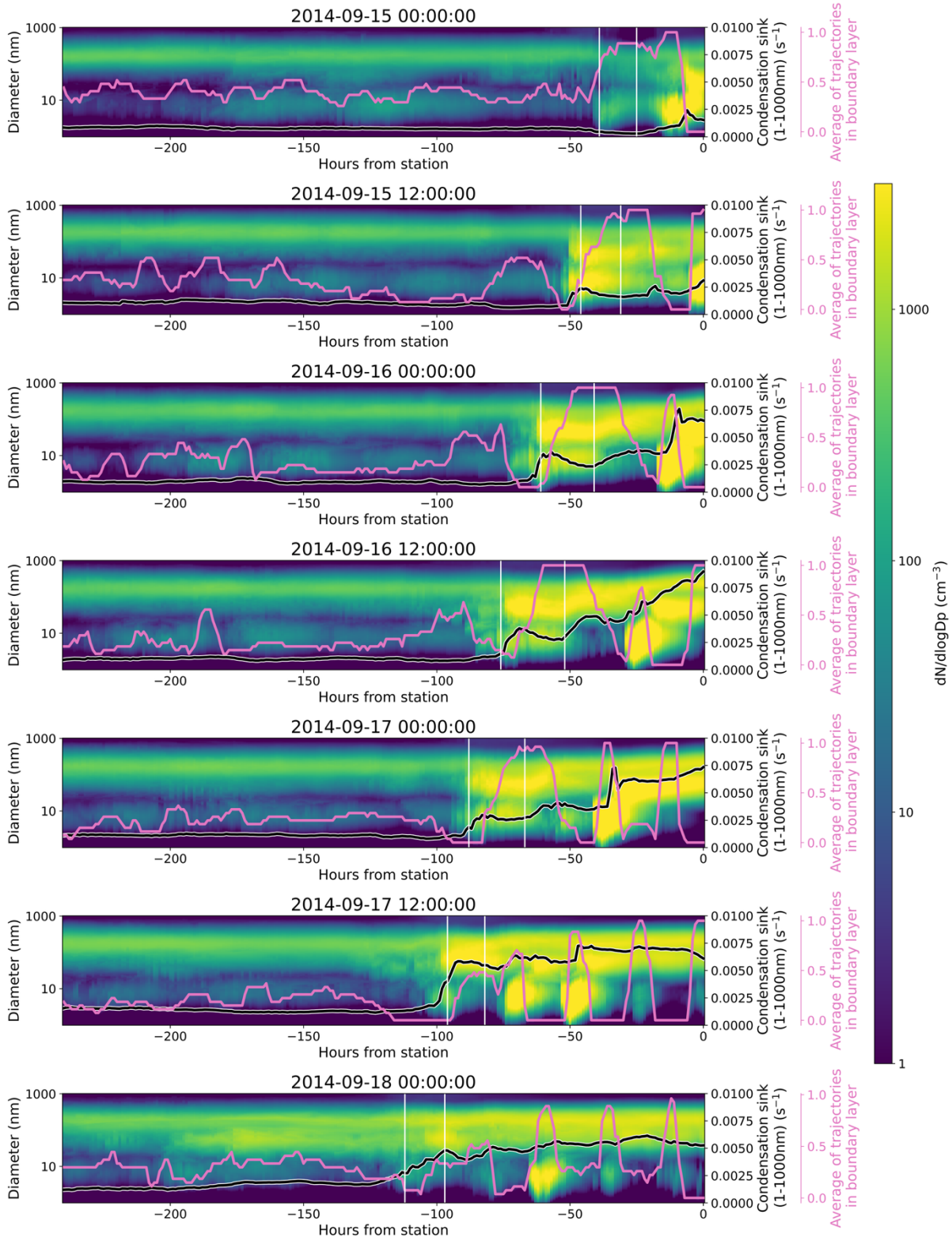


Figure S12: *Timeseries of size distribution in $dN/dlogD_p$ along 10 day back-trajectories originating from Värriö at times from 15th of September 2014 at 12:00, at 12 hourly intervals until the 18th of September at 12:00. Each size distribution for UKESM1.0-BLN. The black line shows the condensation sink for each timestep and the pink line indicates the fraction of the ensemble back-trajectories in the boundary layer starting at each timestep. The white horizontal lines indicate the first portion of consecutive trajectory timesteps (backwards in time) with all ensemble members over ocean.*

2. The trajectory clusters appear to be based mainly on horizontal position and altitude. That is useful for identifying transport pathways, but it is not sufficient by itself to support the microphysical interpretation. Processes such as NPF, condensational growth, sulfate production, and coagulation depend on meteorological history (temperature, RH, vertical velocity, liquid-water exposure, and altitude relative to the boundary layer), not only on position.

I suggest the authors should either provide cluster-wise diagnostics of these variables or test whether the clustering changes when these meteorological variables are included.

We agree with the reviewer that these processes depend on meteorological history as well as position. However, we note that the use of the clusters was employed to sector airmasses that would have had a volcanic influence rather than for separation of conditions for different microphysical processes, and we have added text to highlight this. This approach allows us to separate airmasses arriving from the volcano and perform a characteristic analysis comparing to the climatology at the sites, rather than in-plume out-of-plume analysis as in Peace et al. (2024). We have now calculated the cluster-wise average diagnostics for the suggested variables and provided here, separated into 'volcanically influenced' and non 'volcanically influenced' transport cluster figures (A2-A4). These can identify differences in the meteorology during transport from the eruption compared to other transport locations, which would be expected due to the difference in meteorology and surface of the different transport pathways. As we do not compare the differences in aerosol properties between these cluster sets, we did not feel these figures would contribute greatly to the discussion in the manuscript. We have now also tested the difference in the meteorological variables between the 'volc. year' (2014) and climatology for the clusters used in the study. This is important to isolate the potential differences in meteorology that could lead to differences in the microphysical processes occurring during the eruption period compared to the same locations under standard conditions. We have added the comparison of the climatology and 2014 meteorology to the supplement (Fig. S3-6) and included text in the discussion (see below) as to the influence this could have on the results.

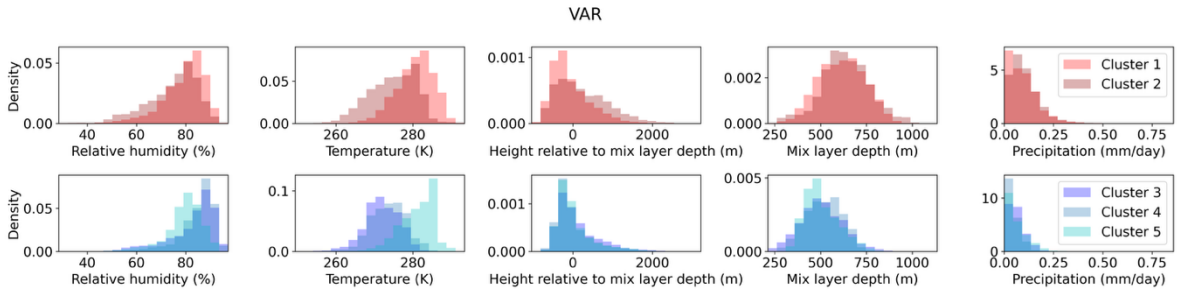


Figure A2: Histograms for each meteorological variable averaged along trajectories arriving at Värriö during September each transport cluster for the climatology period (shades of blue) and volcano period (shades of red). For relative humidity, temperature, mixed layer depth, time in boundary layer and precipitation.

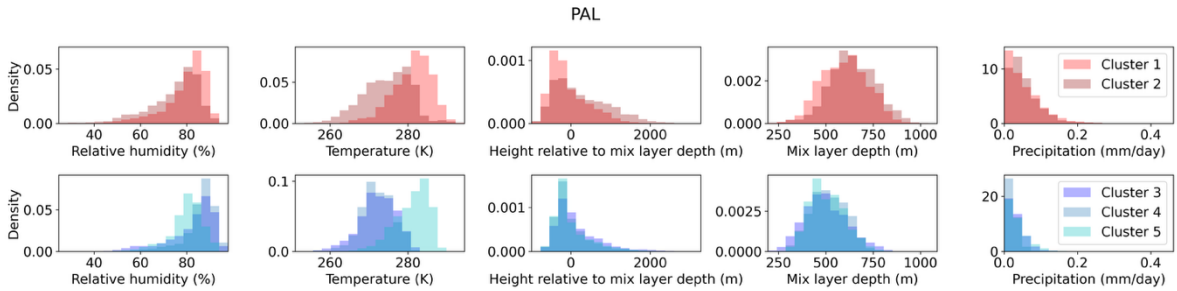


Figure A3: Histograms for each meteorological variable averaged along trajectories arriving at Pallas during September each transport cluster for the climatology period (shades of blue) and volcano period (shades of red). For relative humidity, temperature, mixed layer depth, time in boundary layer and precipitation.

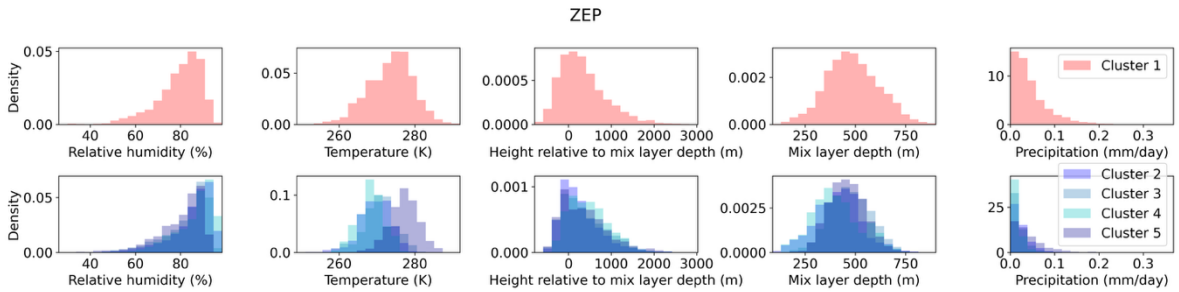


Figure A4: Histograms for each meteorological variable averaged along trajectories arriving at Zeppelin during September each transport cluster for the climatology period (shades of blue) and volcano period (shades of red). For relative humidity, temperature, mixed layer depth, time in boundary layer and precipitation.

Lines 320-343:

'2.8 Cluster meteorology

To isolate any potential confounding changes in meteorology between the eruption period and climatology, we investigate the distributions of average meteorological variables along the ERA-Interim trajectories, for those in the selected transport clusters. There are no notable differences in the distributions between the climatology and volcano for most meteorological variables across the sites (Fig. S3). However, during the volcano year the mixed layer depth is consistently smaller. We hypothesise that this could be due to reduced surface temperatures resulting from both the indirect and direct radiative effects of the Holuhraun plume. For Pallas and Värriö this also corresponds to an increase in trajectory height relative to mixed layer depth, thus an increase in time of trajectories spent in boundary layer, whereas for Zeppelin there is an overall decrease, indicated by the increased mean and median (Fig. S3c). For Pallas and Värriö this could result in more contribution from boundary layer processes during September 2014 compared to the climatology.

The common language effect size (CLES), or probability of superiority was used to test the size of the distribution change (McGraw and Wong, 1992). It is important to note the influence of autocorrelation in this timeseries of overlapping ensemble trajectories, which could impact the performance of statistical significance tests as it breaks the assumption of independent samples. For all variables apart from mixed layer depth these show no effect (defined as 0.5) or small effects (defined as 0.56). Whilst mixed layer depth does show a modest effect (defined as 0.64), the time in boundary layer effect is small (Table S7). We note that the model representation of these changes is different: UKESM variants show no substantial changes in mixed layer depth (Figs. S4 and S5), whereas ECHAM demonstrates significant changes in mixed layer depth (Fig. S6). The perturbation in mixed layer depth could influence the time that the aerosol spends in the boundary layer and whether it overlaps with clouds, thus, impacting the simulated radiative effects. This motivates future Lagrangian studies on the GCM representation of interaction of the plume with clouds.'

S1.5.2 Meteorology in selected clusters

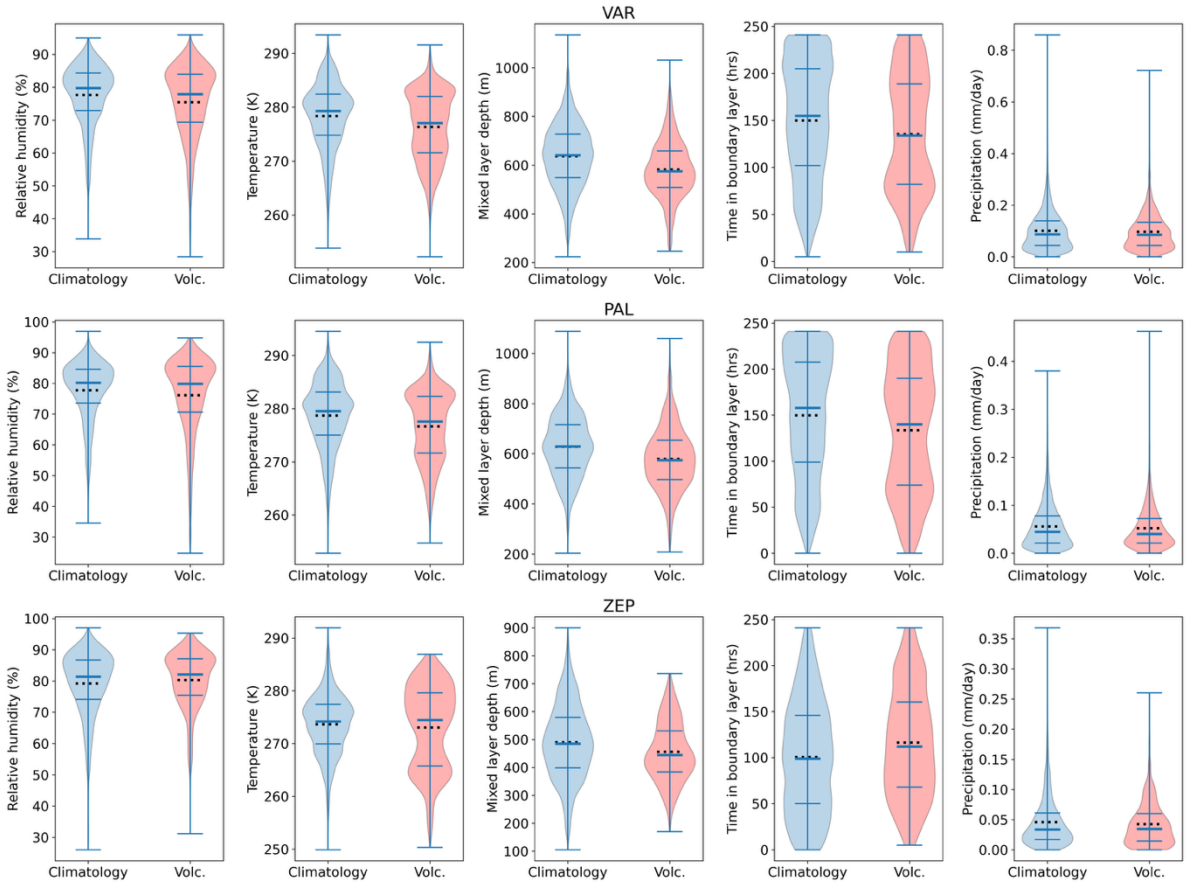


Figure S3: *Violin plots for each meteorological variable averaged along all trajectories arriving at each site during September in the selected transport clusters for the climatology period and volcano period. For relative humidity, temperature, mixed layer depth, time in boundary layer and precipitation as calculated by HYSPLIT for ERA-Interim data. Note that time in boundary layer is the sum of points where the mixed layer depth is high that the trajectory height along the 10-day trajectory, all other variables are calculated as the mean along the 10-day trajectory. The mean is shown for each dataset as the dotted black line.*

	Relative Humidity (%)	***Temperature (K)***	***Mixed layer depth***	***Time in boundary layer (hrs)***	***Precipitation (mm/day)***
Värriö	*0.55*	*0.59*	***0.63***	*0.57*	*0.51*
Pallas	*0.51*	*0.58*	***0.62***	*0.57*	*0.52*
Zeppelin	*0.47*	*0.50*	*0.58*	*0.43*	*0.52*

Table S7: *Testing the size difference in the distribution of the climatology data compared to the eruption data for relative humidity, temperature, mixed layer depth, time in boundary layer and precipitation by using the average common language effect size (CLES). Highlighted values indicate a modest value of CLES.*

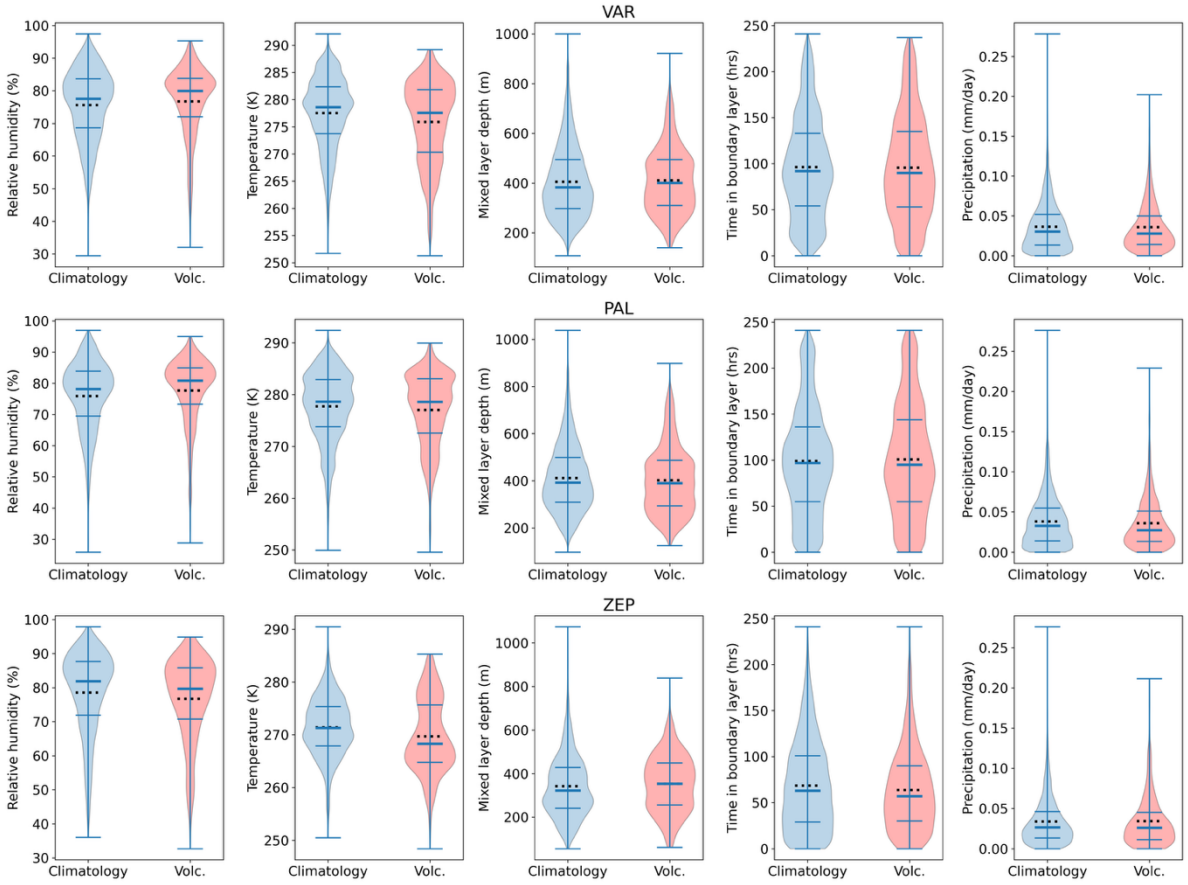


Figure S4: *Violin plots for each meteorological variable averaged along all trajectories arriving at each site during September in the selected transport clusters for the climatology period and volcano period. For relative humidity, temperature, mixed layer depth, time in boundary layer and precipitation as calculated by HYSPLIT for UKESM1.0 data. Note that time in boundary layer is the sum of points where the mixed layer depth is high that the trajectory height along the 10-day trajectory, all other variables are calculated as the mean along the 10-day trajectory. The mean is shown for each dataset as the dotted black line.*

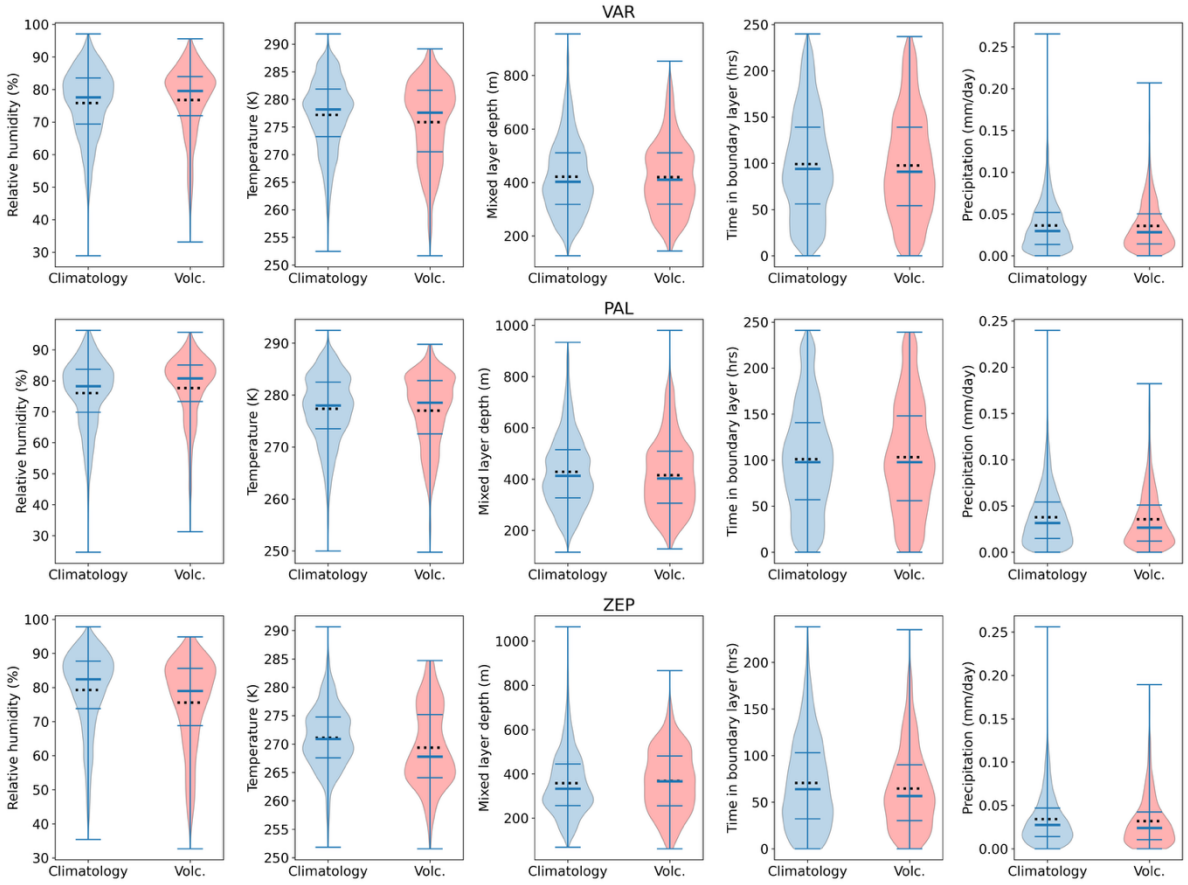


Figure S5: *Violin plots for each meteorological variable averaged along all trajectories arriving at each site during September in the selected transport clusters for the climatology period and volcano period. For relative humidity, temperature, mixed layer depth, time in boundary layer and precipitation as calculated by HYSPLIT for UKESM1.0-BLN10 data. Note that time in boundary layer is the sum of points where the mixed layer depth is high that the trajectory height along the 10-day trajectory, all other variables are calculated as the mean along the 10-day trajectory. The mean is shown for each dataset as the dotted black line.*

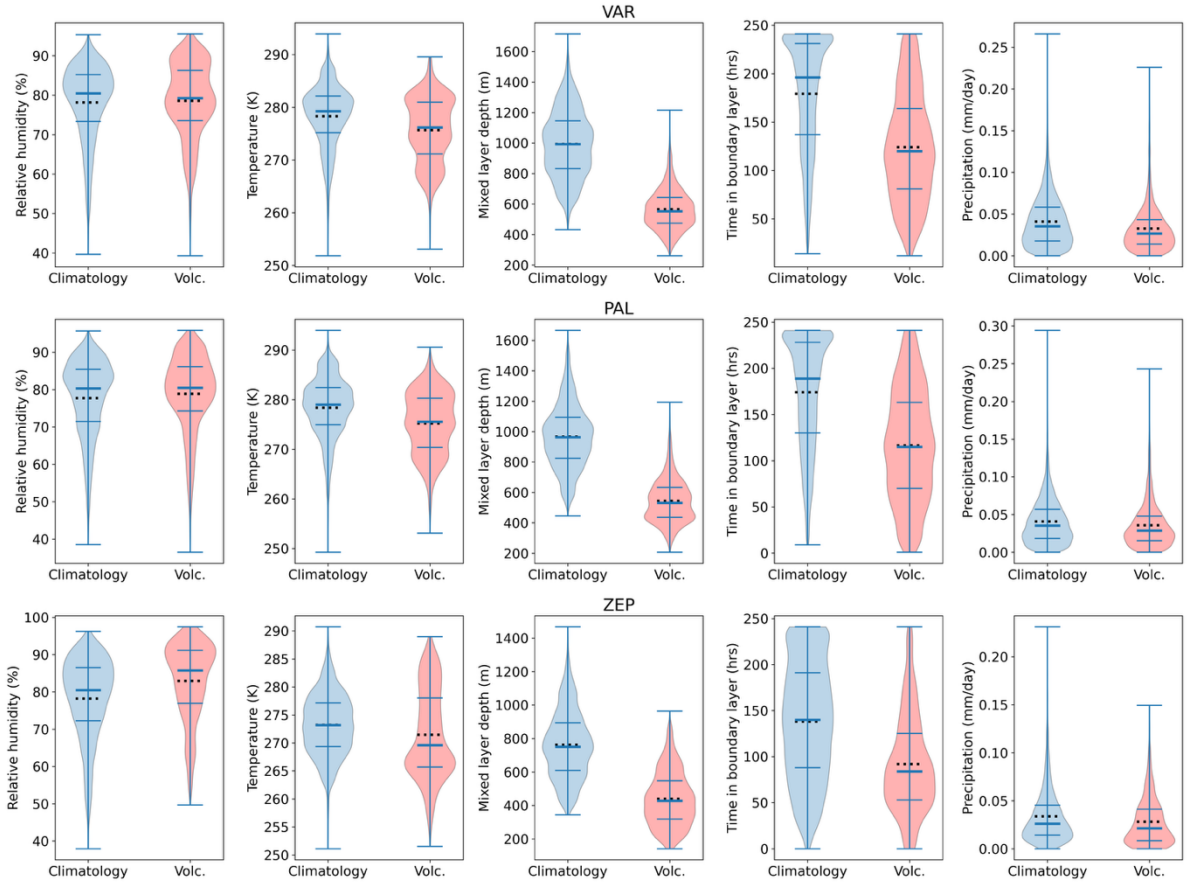


Figure S6: *Violin plots for each meteorological variable averaged along trajectories for all timesteps arriving at Värriö during September in the selected transport clusters for the climatology period and volcano period. For relative humidity, temperature, mixed layer depth, time in boundary layer and precipitation as calculated by HYSPLIT for ECHAM data. Note that time in boundary layer is the sum of points where the mixed layer depth is high that the trajectory height along the 10-day trajectory, all other variables are calculated as the mean along the 10-day trajectory. The mean is shown for each dataset as the dotted black line.*

3. Please clarify how the 27-member trajectory ensemble is used. Is it only used to represent transport uncertainty, or are the individual members treated as independent samples in the cluster statistics?

The individual members are treated as independent samples in the cluster statistics. We have updated the text to make this clearer:

Lines 279-281: *'Clustering was conducted on the entire trajectory timeseries (September 2009-2014 for Pallas and Värriö, September 2010-2014 for Zeppelin) for all ensemble ERA-Interim trajectories, where each ensemble member is treated as an independent sample.'*

4. The BLN effect is currently inferred by visually comparing the two panels in Fig. 6. Since the two UKESM simulations differ only by the inclusion of BLN, a direct UKESM-BLN minus UKESM1.0 difference panel for Δ(dN/dlogDp) would be very helpful. This would show more clearly when BLN adds particles.

Thank you for a suggestion, this is a very useful way to highlight the difference between the two simulations. We have added this as a supplementary figure and included discussion of this figure in Section 3.2:

Lines 475-484: *'This is further highlighted by Figure S7, which shows the difference between the evolution of the modelled size distribution during September 2014 for UKESM and UKESM-BLN for each station. For the*

boreal forest sites UKESM-BLN increases particles in the nucleation and Aitken mode particle number concentrations compared to UKESM, and these particles show clear growth patterns, consistent with growth following a NPF event (i.e. 'banana curves') (Figs. S7a and S7b). There are also increases in accumulation mode number concentrations around 100nm that are particularly notable after the post NPF growth events. At Zeppelin there is a substantial decrease in number for the Aitken mode in UKESM-BLN compared to UKESM on the morning of the 13th of September. This coincides with the peak SO_2 concentration associated with transport from the eruption (Fig. 5) and is followed by a smaller increase in Aitken mode concentration. In general, there is an increase in accumulation mode concentration at Zeppelin for UKESM-BLN compared to UKESM (Fig. S7c).'

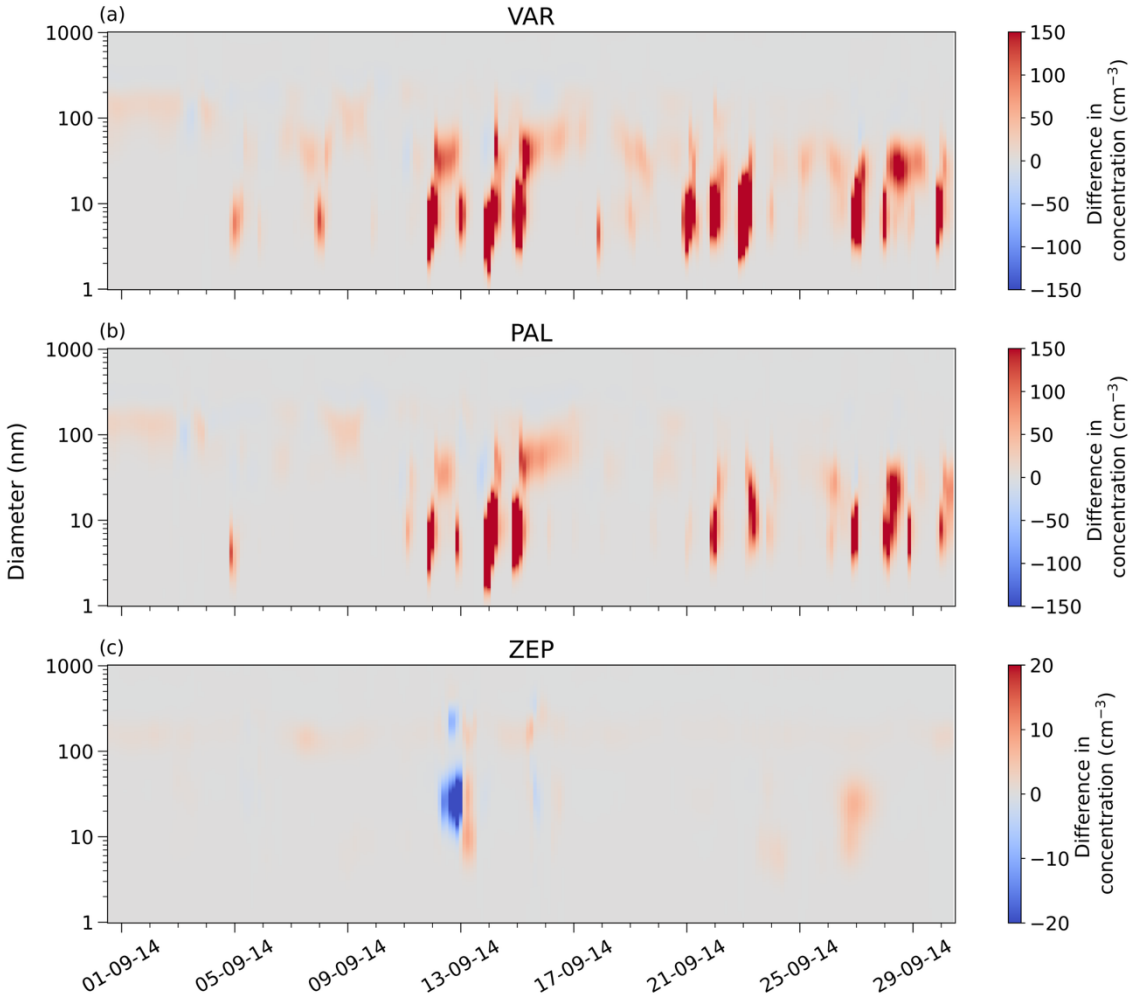


Figure S7: *Timeseries of the difference in size distribution for September 2014 for UKESM1.0-BLN compared to UKESM1.0 in $dN/dlogD_p$. (a) Värriö (b) Pallas and (c) Zeppelin.*

5. If the observations do not resolve particles below approximately 10 nm, then the modeled 1–10 nm nucleation mode and the initial particle formation step cannot be directly validated. In that case, the observational evidence should be described as particle growth consistent with prior or nearby NPF, rather than as direct observational evidence of nucleation.

We agree that this is important to highlight; we have updated the text throughout to make this distinction clearer. For example:

Lines 457-458: *The timings of the observed particle growth consistent with prior or nearby NPF events is well replicated by UKESM-BLN, and there is evidence of sustained growth after the modelled NPF events*

Lines 515-517*: Aitken concentrations are best replicated by ECHAM (Fig. 7a) throughout the eruption period, however, whilst there is evidence of nucleation particles during the eruption period for ECHAM coinciding with the timing of growth after potential NPF events in the observations.*

Lines 540-541: *Results are consistent for Pallas with sustained growth consistent with prior or nearby NPF events observed during the eruption period (Fig. S8a, 14-17th of September),*

6. UKESM-BLN better reproduces the modal-diameter evolution, but it substantially overestimates Aitken-mode number. This raises a key question: is UKESM-BLN producing a more realistic aerosol lifecycle, or is the apparent improvement caused by excessive particle formation being compensated by growth, coagulation, dilution, or deposition? Here, source–sink diagnostics for nucleation, condensational growth, coagulation, and removal would help address this. A tagged volcanic sulfur tracer, if available, would also be valuable for separating plume-derived growth from growth of background aerosol.

Thank you for your comment, in order to investigate this and facilitate comparison between the datasets we have, we added analysis with the derived growth rate of the smallest mode from a bimodal fitting for growth events, condensation sink (10-710nm) and coagulation sink (for 10nm) over (10-710nm). We find that whilst UKESM with the Vehkamäki et al. (2002) parameterisation scheme throughout the boundary layer does exhibit bursts of nucleation mode particles (Fig. 13b), it does not replicate the magnitude or growth stemming from the observations post NPF growth events at the boreal sites (Fig. S13a). ECHAM generates high concentrations of nucleation mode particles but no associated growth into larger sizes indicative of regional NPF (Fig. S13c). The growth rates for the Aitken mode for the particularly long lived post-NPF growth events identified in the observations (15-18th of September and 18th-20th) were calculated. UKESM-BLN closely replicated the observed growth rates (Table S10). The coagulation sink was found to be best replicated by UKESM, as well as the condensation sink (Fig. S14a). It is clear that whilst UKESM better represents the coagulation and condensation sink terms, it does not accurately reproduce the impact of the eruption on the physical characteristics of the aerosol particle number size distributions at any site (Fig. 8), suggesting missing processes. We do not have a tagged volcanic sulphur tracer available from the simulations, instead we are able to use collocation of sulphur onto the trajectories to identify the location of the plume and clustering to isolate transport from the eruption site.

We have added the following text and figures to discuss these additional diagnostics:

Lines 371-383: *The coagulation sink is a measure of how quickly smaller aerosol particles are lost to coagulation with the larger pre-existing aerosol population (Dal Maso, 2002). The coagulation sink is defined for a specific aerosol size (in this study 10nm) and is defined as:*

$$CoagS_i = \sum_j K(D_{p,i}, D_{p,j}) N_j \quad (6)$$

Where $K(D_{p,i}, D_{p,j})$ is the coagulation coefficient for a particle of size i, with background particle of size j. Herein, condensation and coagulation sink will be used to refer to the condensation and coagulation (for 10nm) sinks of aerosol particles over the size range 10nm to the site upper measurement limit included in this study (Table 3).

To calculate the growth rate, a bi-modal fitting of the full (1-1000nm) size distributions for each dataset was performed using an adaptation of the python implementation of the DOFIT algorithm (Khadir, 2023). The change in diameter of the smallest fitted mode was then calculated over the duration of the identified post NPF growth event (Eq. 7) (Kulmala et al., 2012).

$$GR = \frac{\Delta D_m}{\Delta t} \quad (7)$$

Lines 508-514: *'The growth rates for the Aitken mode for particularly long lived post-NPF growth events in the observations (15-18th of September and 18th-20th) were calculated finding similar results for UKESM-BLN as in the observations (Table S10). Whilst UKESM with the Vehkamäki et al. (2002) nucleation scheme throughout the boundary layer does exhibit bursts of nucleation mode particles (Fig. S13b) and closely matches the observed coagulation sink (10nm) (Fig. S12b) and condensation sink (Fig. S14a), it does not replicate the magnitude or growth stemming from the observations post NPF growth events (Fig. S13a, Table S10), highlighting the importance of the organic-mediated boundary layer nucleation parameterisation.'*

Lines 515-519: *'Aitken concentrations are best replicated by ECHAM (Fig. 7a) throughout the eruption period, however, whilst there is evidence of nucleation particles during the eruption period for ECHAM coinciding with the timing of growth after potential NPF events in the observations. There is no continuous growth from the nucleation mode to larger modes (Fig. 6d), as observed (Fig. 6a). ECHAM exhibits much lower growth rates compared to observations (Table S10), despite a much lower condensation and coagulation sink compared to the other models and the observations (Figs. 12a and 12b).'*

S2.4 Growth rate results

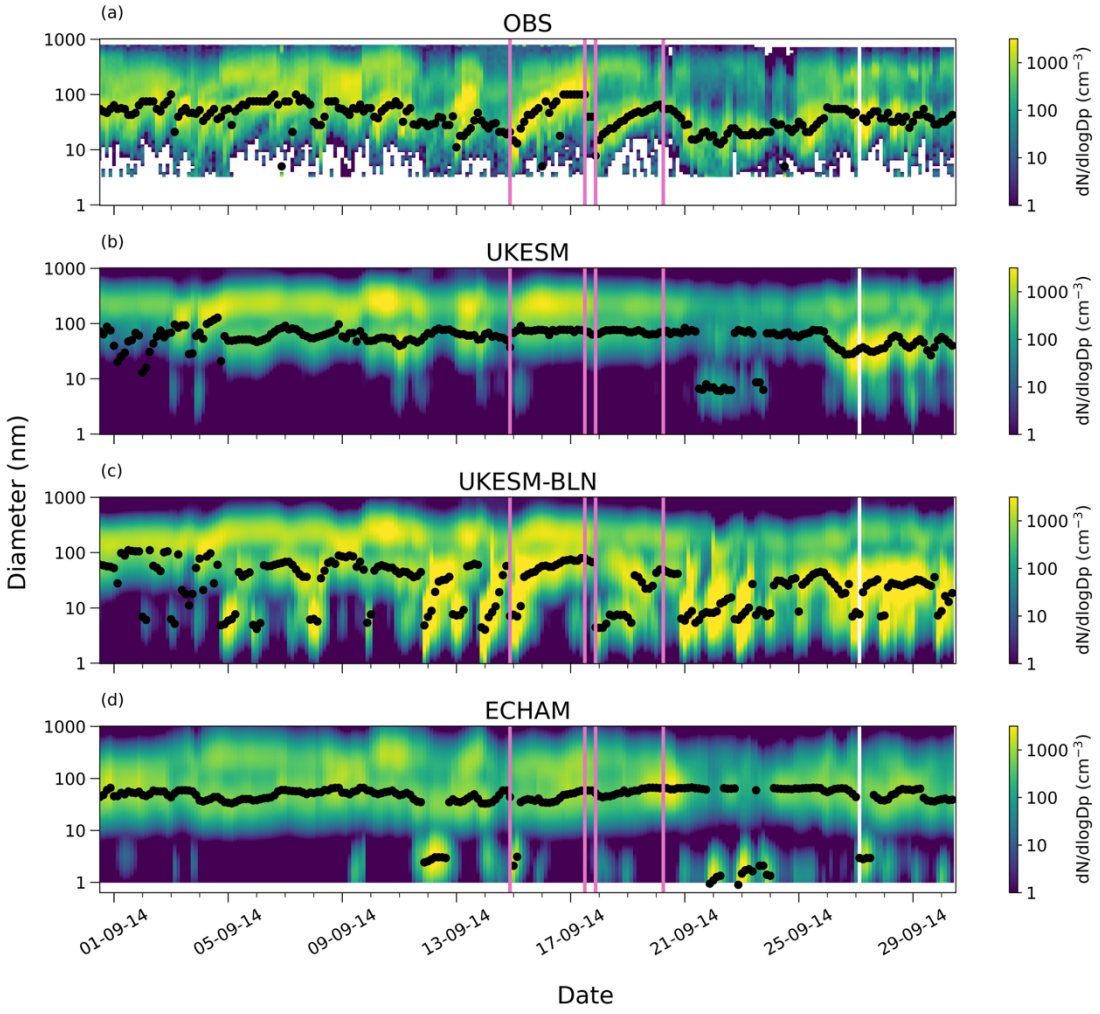


Figure S13: *Timeseries of size distribution for September 2014 at Värriö in dN/dlogD$_p$. (a) observations (DMPS), (b) UKESM1.0, (c) UKESM1.0-BLN and (d) ECHAM6.3HAM2.3. The black points indicate the first modal diameter from a bimodal fitting. The pink vertical lines indicate the post NPF growth events identified to investigate the growth rate.*

	Average growth rate (nm/hr) for the event: 15th of September at 09:00 -18th of September at 00:00	***Average growth rate (nm/hr) for the event: 18th of September at 09:00 - 20th of September at 18:00***
Observations	*1.25*	*0.82*
UKESM	*0.57*	*0.07*
UKESM-BLN	*1.14*	*0.79*
ECHAM	*0.24*	*0.25*

Table S10: *The growth rates of the first mode from a bimodal fitting (Fig. S13) for two post-NPF growth events for each dataset.*

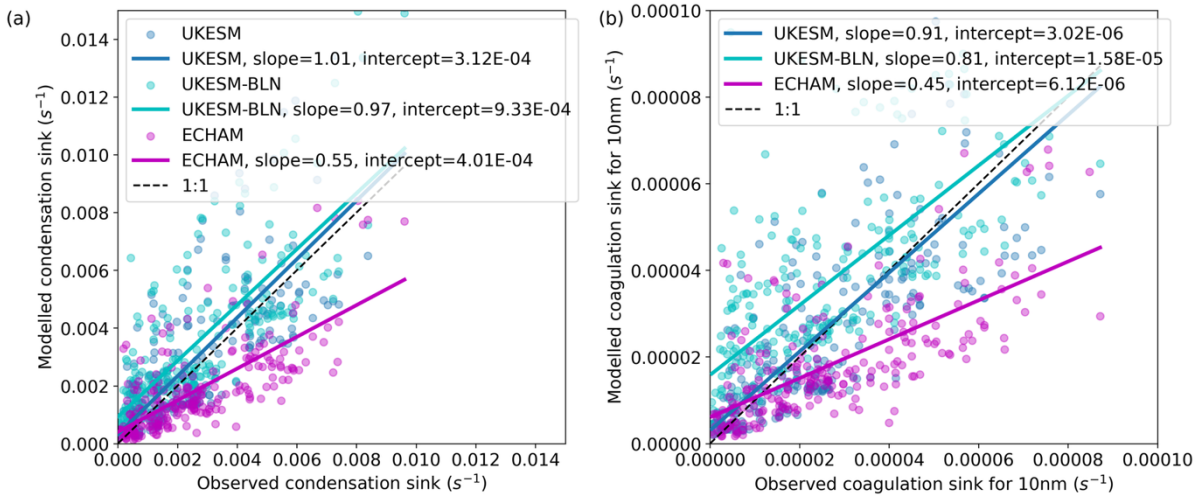


Figure S14: *(a) The observed condensation sink (10-710nm) compared to the modelled condensation sink (10-710nm) for each timestep for Värriö, for each model with UKESM1.0 (blue), UKESM1.0-BLN (cyan) and ECHAM6.3-HAM2.3 (magenta). The linear fits are given in each model colour respectively. The 1:1 line is represented by the black dashed line. (b) As (a) but for the coagulation sink for 10nm.*

Minor comments

-Line 185: “The simulations of the eruption at Holuhraun in 2014 use emission altitude and magnitude described by Malavelle et al. (2017), distributed between the 800 m and 3000 km”- is this a typo? Should this be 3000 m rather than 3000 km?

Thank you for noting this typo. This has been corrected in the manuscript.

-Please clarify whether the UKESM-BLN improvements are statistically significant across the three sites, size ranges, and trajectory clusters, or whether they are mainly limited to specific transport regimes.

Thank you for your comment. We note that UKESM-BLN does not show a consistent improvement in absolute numbers of aerosol for the boreal sites demonstrated by the NMBF analysis, it is the representation of the volcanic perturbation in which we see the improvement. We have included a Diebold-Mariano statistical test with the NMBF analysis for each site and size range comparing the three model predictions pairwise at three-hourly resolution which demonstrates that the magnitude of concentrations with the Metzger nucleation scheme is too high.

In UKESM-BLN the growth rates and changes in size distribution associated with the eruption are more consistent with the observed processes. We find that the perturbation in potential CCN (N80) is better replicated by UKESM-BLN compared at the Boreal sites (Figs. 14, 15 and S17 and S18) and the RMSE is lower (Table S11). This is consistent across transport regimes – particularly from the volcano which is the focus of this study. We cannot add significance testing on the CWT N80 maps as the delta is calculated from the averaged CWT maps as we are comparing different periods of time. We have included the regression figures for the other sites in the supplement (Figs. S22 and S23), and the root mean squared error (Table S11) for each to demonstrate more clearly the improvement.

We have added a description of the statistical test implementation, figures and tables of results to the supplement and text discussing the results:

Lines 354-360:
‘2.10 Diebold Mariano

The Diebold Mariano test compares the predictive power of two forecasts (Diebold and Mariano, 1995). In this study it is used to compare the predictive power of each of the model predictions for Aitken mode, accumulation mode and total concentrations at 3-hourly resolution compared to the observations at each site during September 2014. We utilise the python implementation in the diboldmariano package (dieboldmariano · PyPI, 2026) with the Harvey, Leybourne and Newbold correction for small samples (Harvey et al., 1998).

Lines 458-475: However, despite the inclusion of the reduced boundary layer nucleation rate (Ranjithkumar et al., 2021), the concentrations associated with the NPF events in UKESM-BLN lead to total concentrations (for D_p=10-710nm) that are an average factor of 1.98 too high over September (Table S8). Some post-NPF growth events, for example the 12th of September and 22nd of September lead to NMBF in the total aerosol concentration (for D_p=10-710nm) of up to 10, demonstrating a very high bias for UKESM-BLN (Figs. 7a and 7c). The high bias of UKESM-BLN is further confirmed by the Diebold Mariano tests which demonstrate that the magnitude of concentrations is significantly better represented by UKESM for Aitken and total concentrations at the boreal sites (Table S9).
In general, UKESM and ECHAM underpredict total aerosol number concentrations at Värriö (Fig. 7c) by average factors of 1.67 and 1.77 respectively (Table S8). ECHAM significantly outperforms both UKESM variants for Aitken mode predictions (Table S9), and compared to UKESM-BLN, ECHAM significantly better replicated concentrations for almost all sites and size ranges (Table S9). UKESM substantially underpredicts the Aitken mode on a daily timescale, with a maximum absolute NMBF of 37.2 (Fig. 7a), but on average overpredicts the accumulation mode (Fig. 7b). Introducing organic-mediated BLN in UKESM-BLN, results in reduced underprediction from the daily NMBF for the Aitken mode concentrations (Fig. 7a), but increased overprediction of the accumulation mode concentrations (Fig. 7b), emphasising the contribution of the organic-mediated BLN to all lognormal aerosol modes in UKESM. However, even with the reduction of the nucleation

rate following Ranjithkumar et al. (2021), there is still a substantial overprediction from the addition of the Metzger et al. (2010) scheme in UKESM and we suggest further tuning could be explored in future studies.'

***Lines: 903-907**: 'Both UKESM and ECHAM substantially underpredict the climatology (Fig. S22a and b), which leads to over prediction of the ΔN80. UKESM-BLN overpredicts N80 for both the climatology and volcano period (Fig. S22), this results in an overall lower RMSE and shows that UKESM-BLN (200.21) represents an improvement in representing the perturbation at Värriö compared to UKESM (265.30), however ECHAM demonstrates the lowest overall RMSE (150.72) (Table S11).'*

***Lines 916-919:** 'Comparing to the other sites, we find consistent results for Pallas in the spatial distribution of the plume (Fig. S20). However, we note that for Pallas the size limit to include in the CCN approximation, is much lower (430nm) compared to the other sites. UKESM-BLN best replicates the spatial distribution of the ΔN80 of the plume but overestimates the ΔN80 (Figs. S20c, S20i and S22).'*

	Värriö			**Pallas**			**Zeppelin**		
	N10-100nm	**N100-710nm**	**N10-710nm**	**N10-100nm**	**N100-430nm**	**N10-430nm**	**N10-100nm**	**N100-630nm**	**N10-630nm**
UKESM and UKESM-BLN	**2.56×10^{-4}**	**0.45**	**1.39×10^{-4}**	**0.01**	**2.57×10^{-3}**	**5.92×10^{-3}**	0.96	**0.01**	0.97
UKESM-BLN and UKESM	1.00	0.56	1.000	0.99	1.00	0.99	**0.04**	0.99	**0.03**
UKESM and ECHAM	0.97	0.99	**0.04**	0.95	1.00	0.11	0.99	0.75	0.96
ECHAM and UKESM	**0.03**	**0.01**	0.96	**0.05**	**1.83×10^{-6}**	0.89	**5.31×10^{-3}**	0.25	**0.04**
UKESM-BLN and ECHAM	1.00	0.98	1.00	0.99	1.00	0.99	0.99	0.73	0.92
ECHAM and UKESM-BLN	**2.06×10^{-4}**	**0.02**	**2.14×10^{-4}**	**0.01**	**3.38×10^{8}**	**7.97×10^{-3}**	**0.01**	**0.22**	**0.08**

Table S9: Diebold Mariano p-values for the timeseries of in a pairwise comparison with the first of the listed pair being assumed to be less than in the other model (thus, closer to the observations), statistically significant at the 5% level are indicated by bold font.

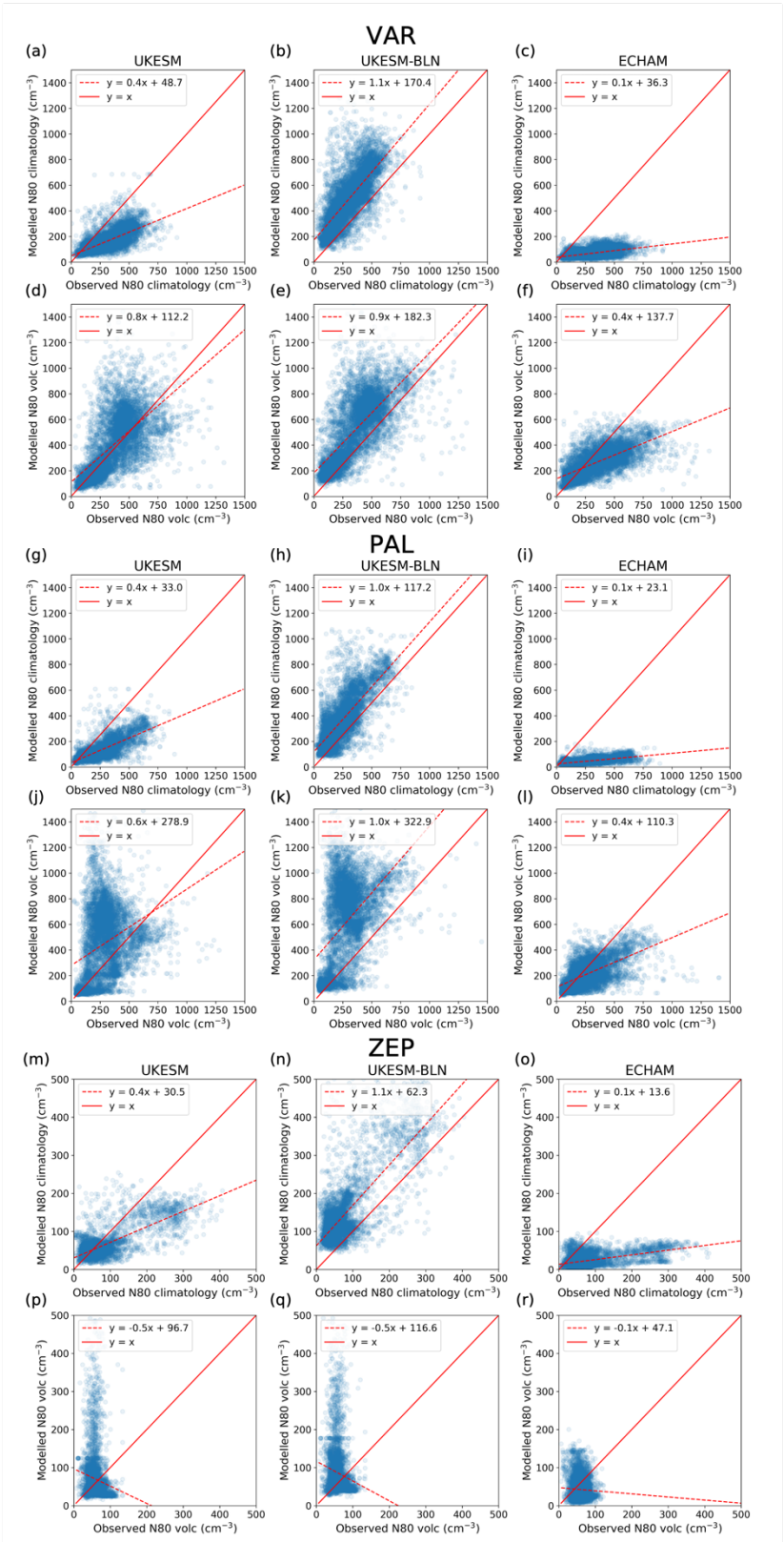


Figure S22: The mean per grid cell N80, utilising the concentration weighted trajectory (CWT) model (Eq. 2, Fig. 14) for DMPS with ERA-Interim compared to UKESM1.0 (a, d, g, j, m and p), UKESM1.0-BLN10 (b, e, h, k, n and q) and ECHAM6.3-HAM2.3 (c, f, i, l ,o and p). For the climatology (a-c, g-I and m-o) and the volcano period (d-f, j-l and p-r) at *Värriö* (a-f), Pallas (g-l) and Zeppelin (m-r). The solid red line indicates a 1:1 match and the dashed red line gives the regression between the two datasets. Note the difference in y-axis limits between subfigures, but consistent within subfigures. Note that these figures demonstrate all points across the trajectory domain, beyond the focused region of Fig. 14, S20 and S21.

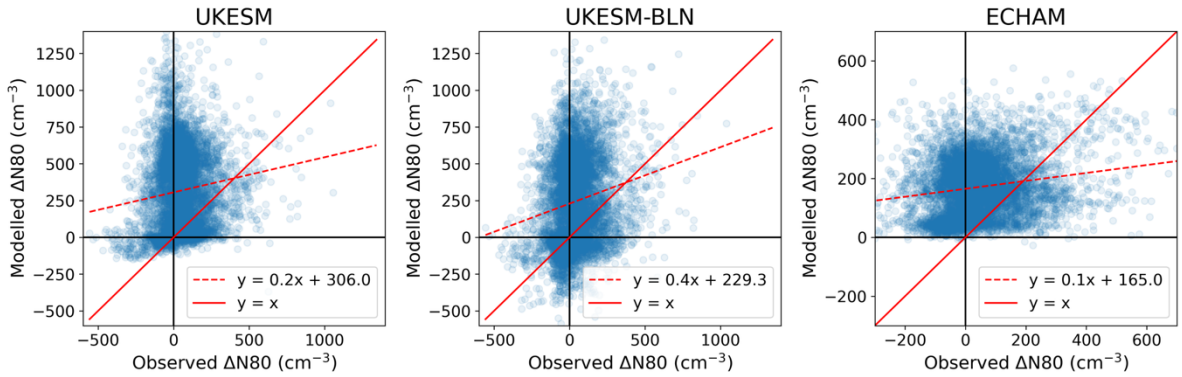


Figure S22: The mean per grid cell for the difference (volcanic period minus climatology) in concentration for Pallas, utilising the concentration weighted trajectory (CWT) model (Eq. 2, Fig. 14) for DMPS with ERA-Interim compared to UKESM1.0 (a), UKESM1.0-BLN10 (b) and ECHAM6.3-HAM2.3 (c). The solid red line indicates a 1:1 match and the dashed red line gives the regression between the two datasets. Note the difference in y-axis limits between subfigures, but consistent within subfigures. Note that these figures demonstrate all points across the trajectory domain, beyond the focused region of Fig. S20.

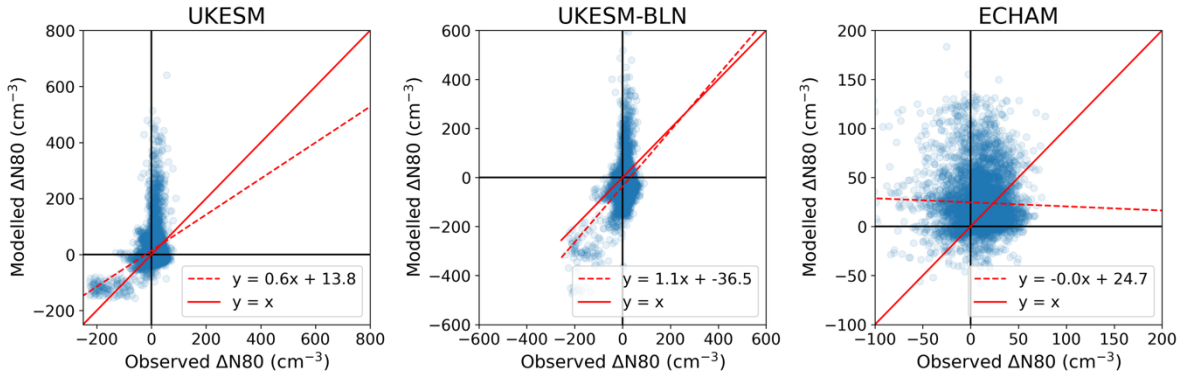


Figure S23: The mean per grid cell for the difference (volcanic period minus climatology) in concentration for Zeppelin, utilising the concentration weighted trajectory (CWT) model (Eq. 2, Fig. 14) for DMPS with ERA-Interim compared to UKESM1.0 (a), UKESM1.0-BLN10 (b) and ECHAM6.3-HAM2.3 (c). The solid red line indicates a 1:1 match and the dashed red line gives the regression between the two datasets. Note the difference in y-axis limits between subfigures, but consistent within subfigures. Note that these figures demonstrate all points across the trajectory domain, beyond the focused region of Fig. S21.

	Värriö	Pallas	Zeppelin
UKESM1.0	265.30	401.98	68.07
UKESM1.0-BLN10	200.21	366.67	81.14
ECHAM6.3-HAM2.3	150.72	194.73	40.95

Table S11: The root mean squared error (observations compared to model) for the CWT model derived difference (volcanic period minus climatology) in concentration, corresponding to Figs. 15, S22 and S23.

References

Lampilahti, J. et al. Zeppelin-led study on the onset of new particle formation in the planetary boundary layer. ACP, 21, no. 16 (2021): 12649-12663. https://doi.org/10.5194/acp-21-12649-2021

Metzger, A. et al. Evidence for the role of organics in aerosol particle formation under atmospheric conditions. PNAS, 107, no. 15 (2010): 6646-6651

Citation: https://doi.org/10.5194/egusphere-2026-1043-RC2

Additional updates

Text has had minor adjustments to improve clarity. We found that trajectories for the day of the 30/09/2009 were missing from original analysis so these have been added and the figures and tables have been updated throughout. There was a minor bug in the calculation of the condensation sink which has now been updated, this has resulted in small changes in magnitude of the condensation sink but no changes in the relative magnitude between observations and models, thus, no change to results. We have also removed the largest three bins from the calculation of accumulated variables Värriö to ensure a more robust comparison to the GCMs as there is missing observational data during September 2014 in the 731-784nm size ranges (Fig. 6a). This has no significant impact on results.

Lines 166-170: *'We note that for September 2014 there is some missing data throughout the Värriö timeseries in the highest 3 size bins 731-784nm (Fig. 6a), therefore in order to facilitate the most robust comparison to the GCMs we remove these bins for comparisons of accumulated variables such as concentrations, condensation sink and coagulation sink, thus starting our size range at 710nm.'*

References

Alam, A., Shi, J. P., and Harrison, R. M.: Observations of new particle formation in urban air, Journal of Geophysical Research: Atmospheres, 108, https://doi.org/10.1029/2001JD001417, 2003.

Asmi, E., Kivekäs, N., Kerminen, V.-M., Komppula, M., Hyvärinen, A.-P., Hatakka, J., Viisanen, Y., and Lihavainen, H.: Secondary new particle formation in Northern Finland Pallas site between the years 2000 and 2010, Atmos. Chem. Phys, 11, 12959–12972, https://doi.org/10.5194/acp-11-12959-2011, 2011.

Boulon, J., Sellegri, K., Hervo, M., and Laj, P.: Observations of nucleation of new particles in a volcanic plume, Proc. Natl. Acad. Sci. U. S. A., 108, 12223–12226, https://doi.org/10.1073/PNAS.1104923108/, 2011.

Bousiotis, D., Pope, F. D., Beddows, D. C. S., Dall'Osto, M., Massling, A., Nøjgaard, J. K., Nordstrøm, C., Niemi, J. V., Portin, H., Petäjä, T., Perez, N., Alastuey, A., Querol, X., Kouvarakis, G., Mihalopoulos, N., Vratolis, S., Eleftheriadis, K., Wiedensohler, A., Weinhold, K., Merkel, M., Tuch, T., and Harrison, R. M.: A phenomenology of new particle formation (NPF) at 13 European sites, Atmos. Chem. Phys., 21, 11905–11925, https://doi.org/10.5194/ACP-21-11905-2021, 2021.

Dal Maso, M.: Condensation and coagulation sinks and formation of nucleation mode particles in coastal and boreal forest boundary layers, J. Geophys. Res., 107, 8097, https://doi.org/10.1029/2001JD001053, 2002.

Diebold, F. X. and Mariano, R. S.: Comparing Predictive Accuracy, Journal of Business & Economic Statistics, 13, 253, https://doi.org/10.2307/1392185, 1995.

Harvey, D. I., Leybourne, S. J., and Newbold, P.: Tests for Forecast Encompassing, Journal of Business & Economic Statistics, 16, 254, https://doi.org/10.2307/1392581, 1998.

Heikkinen, L., Partridge, D. G., Blichner, S., Huang, W., Ranjan, R., Bowen, P., Tovazzi, E., Petäjä, T., Mohr, C., and Riipinen, I.: Cloud response to co-condensation of water and organic vapors over the boreal forest, Atmos. Chem. Phys, 24, 5117–5147, https://doi.org/10.5194/acp-24-5117-2024, 2024.

Horowitz, L. W., Walters, S., Mauzerall, D. L., Emmons, L. K., Rasch, P. J., Granier, C., Tie, X., Lamarque, J. F., Schultz, M. G., Tyndall, G. S., Orlando, J. J., and Brasseur, G. P.: A global simulation of tropospheric ozone and related tracers: Description and evaluation of MOZART, version 2, Journal of Geophysical Research: Atmospheres, 108, 4784, https://doi.org/10.1029/2002JD002853, 2003.

Inness, A., Baier, F., Benedetti, A., Bouarar, I., Chabrillat, S., Clark, H., Clerbaux, C., Coheur, P., Engelen, R. J., Errera, Q., Flemming, J., George, M., Granier, C., Hadji-Lazaro, J., Huijnen, V., Hurtmans, D., Jones, L., Kaiser,

J. W., Kapsomenakis, J., Lefever, K., Leitão, J., Razinger, M., Richter, A., Schultz, M. G., Simmons, A. J., Suttie, M., Stein, O., Thépaut, J. N., Thouret, V., Vrekoussis, M., and Zerefos, C.: The MACC reanalysis: An 8 yr data set of atmospheric composition, Atmos. Chem. Phys., 13, 4073–4109, https://doi.org/10.5194/ACP-13-4073-2013, 2013.

Jang, S., Park, K. T., Lee, K., Yoon, Y. J., Kim, K., Chung, H. Y., Jang, E., Becagli, S., Lee, B. Y., Traversi, R., Eleftheriadis, K., Krejci, R., and Hermansen, O.: Large seasonal and interannual variations of biogenic sulfur compounds in the Arctic atmosphere (Svalbard; 78.9g N, 11.9g E), Atmos. Chem. Phys., 21, 9761–9777, https://doi.org/10.5194/ACP-21-9761-2021, 2021.

Jokinen, T., Lehtipalo, K., Thakur, R. C., Ylivinkka, I., Neitola, K., Sarnela, N., Laitinen, T., Kulmala, M., Petäjä, T., and Sipilä, M.: Measurement report: Long-term measurements of aerosol precursor concentrations in the Finnish subarctic boreal forest, Atmos. Chem. Phys., 22, 2237–2254, https://doi.org/10.5194/ACP-22-2237-2022, 2022.

Kazil, J., Stier, P., Zhang, K., Quaas, J., Kinne, S., O'Donnell, D., Rast, S., Esch, M., Ferrachat, S., Lohmann, U., and Feichter, J.: Aerosol nucleation and its role for clouds and Earth's radiative forcing in the aerosol-climate model ECHAM5-HAM, Atmos. Chem. Phys., 10, 10733–10752, https://doi.org/10.5194/ACP-10-10733-2010, 2010.

Khadir, T.: Particle_Size_Distribution_Log_Fit_Python: Particle_Size_Distribution_Log_Fit_Python, https://doi.org/10.5281/ZENODO.8017043, 2023., 2023.

Kulmala, M., Petäjä, T., Nieminen, T., Sipilä, M., Manninen, H. E., Lehtipalo, K., Dal Maso, M., Aalto, P. P., Junninen, H., Paasonen, P., Riipinen, I., Lehtinen, K. E. J., Laaksonen, A., and Kerminen, V. M.: Measurement of the nucleation of atmospheric aerosol particles, Nat. Protoc., 7, 1651–1667, https://doi.org/10.1038/NPROT.2012.091, 2012.

Leinonen, V., Kokkola, H., Yli-Juuti, T., Mielonen, T., Kühn, T., Nieminen, T., Heikkinen, S., Miinalainen, T., Bergman, T., Carslaw, K., Decesari, S., Fiebig, M., Hussein, T., Kivekäs, N., Krejci, R., Kulmala, M., Leskinen, A., Massling, A., Mihalopoulos, N., Mulcahy, J. P., Noe, S. M., Van Noije, T., O'connor, F. M., O'dowd, C., Olivie, D., Pernov, J. B., Petäjä, T., Seland, Ø., Schulz, M., Scott, C. E., Skov, H., Swietlicki, E., Tuch, T., Wiedensohler, A., Virtanen, A., and Mikkonen, S.: Comparison of particle number size distribution trends in ground measurements and climate models, Atmos. Chem. Phys., 22, 12873–12905, https://doi.org/10.5194/ACP-22-12873-2022, 2022.

McGraw, K. O. and Wong, S. P.: A common language effect size statistic., Psychol. Bull., 111, 361–365, https://doi.org/10.1037/0033-2909.111.2.361, 1992.

Metzger, A., Verheggen, B., Dommen, J., Duplissy, J., Prevot, A. S. H., Weingartner, E., Riipinen, I., Kulmala, M., Spracklen, D. V., Carslaw, K. S., and Baltensperger, U.: Evidence for the role of organics in aerosol particle formation under atmospheric conditions, Proc. Natl. Acad. Sci. U. S. A., 107, 6646–6651, https://doi.org/10.1073/PNAS.0911330107, 2010.

Peace, A. H., Chen, Y., Jordan, G., Partridge, D. G., Malavelle, F., Duncan, E., and Haywood, J. M.: In-plume and out-of-plume analysis of aerosol–cloud interactions derived from the 2014–2015 Holuhraun volcanic eruption, Atmos. Chem. Phys., 24, 9533–9553, https://doi.org/10.5194/ACP-24-9533-2024, 2024.

Ranjithkumar, A., Gordon, H., Williamson, C., Rollins, A., Pringle, K., Kupc, A., Luke Abraham, N., Brock, C., and Carslaw, K.: Constraints on global aerosol number concentration, SO2and condensation sink in UKESM1 using ATom measurements, Atmos. Chem. Phys., 21, 4979–5014, https://doi.org/10.5194/ACP-21-4979-2021, 2021.

Sellar, A. A., Jones, C. G., Mulcahy, J. P., Tang, Y., Yool, A., Wiltshire, A., O'Connor, F. M., Stringer, M., Hill, R., Palmieri, J., Woodward, S., de Mora, L., Kuhlbrodt, T., Rumbold, S. T., Kelley, D. I., Ellis, R., Johnson, C. E., Walton, J., Abraham, N. L., Andrews, M. B., Andrews, T., Archibald, A. T., Berthou, S., Burke, E., Blockley, E., Carslaw, K., Dalvi, M., Edwards, J., Folberth, G. A., Gedney, N., Griffiths, P. T., Harper, A. B., Hendry, M. A., Hewitt, A. J., Johnson, B., Jones, A., Jones, C. D., Keeble, J., Liddicoat, S., Morgenstern, O., Parker, R. J., Predoi, V., Robertson, E., Siahaan, A., Smith, R. S., Swaminathan, R., Woodhouse, M. T., Zeng, G., and

Zerroukat, M.: UKESM1: Description and Evaluation of the U.K. Earth System Model, J. Adv. Model. Earth Syst., 11, 4513–4558, https://doi.org/10.1029/2019MS001739, 2019.

Stier, P., Feichter, J., Kinne, S., Kloster, S., Vignati, E., Wilson, J., Ganzeveld, L., Tegen, I., Werner, M., Balkanski, Y., Schulz, M., Boucher, O., Minikin, A., and Petzold, A.: The aerosol-climate model ECHAM5-HAM, Atmos. Chem. Phys., 5, 1125–1156, https://doi.org/10.5194/ACP-5-1125-2005, 2005.

Vehkamäki, H., Kulmala, M., Napari, I., Lehtinen, K. E. J., Timmreck, C., Noppel, M., and Laaksonen, A.: An improved parameterization for sulfuric acid–water nucleation rates for tropospheric and stratospheric conditions, Journal of Geophysical Research: Atmospheres, 107, AAC 3-1, https://doi.org/10.1029/2002JD002184, 2002.

Vehkamäki, H., Dal Maso, M., Hussein, T., Flanagan, R., Hyvärinen, A., Lauros, J., Merikanto, J., Mönkkönen, P., Pihlatie, M., Salminen, K., Sogacheva, L., Thum, T., Ruuskanen, T. M., Keronen, P., Aalto, P. P., Hari, P., Lehtinen, K. E. J., Rannik, ¨ U, and Kulmala, M.: Atmospheric Chemistry and Physics Atmospheric particle formation events at Värriö measurement station in Finnish Lapland 1998-2002, Atmos. Chem. Phys, 4, 2015.

Virtanen, A., Joutsensaari, J., Kokkola, H., Partridge, D. G., Blichner, S., Seland, Ø., Holopainen, E., Tovazzi, E., Lipponen, A., Mikkonen, S., Leskinen, A., Hyvärinen, A.-P., Zieger, P., Krejci, R., Ekman, A. M. L., Riipinen, I., Quaas, J., and Romakkaniemi, S.: High sensitivity of cloud formation to aerosol changes, Nat. Geosci., 18, 289–295, https://doi.org/10.1038/s41561-025-01662-y, 2025.

Zhang, K., O'donnell, D., Kazil, J., Stier, P., Kinne, S., Lohmann, U., Ferrachat, S., Croft, B., Quaas, J., Wan, H., Rast, S., and Feichter, J.: The global aerosol-climate model ECHAM-HAM, version 2: sensitivity to improvements in process representations, Atmos. Chem. Phys, 12, 8911–8949, https://doi.org/10.5194/acp-12-8911-2012, 2012.

dieboldmariano · PyPI, https://pypi.org/project/dieboldmariano/, last access: 7 October 2026., 2026.